The Thesis committee for Alokraj Valsaraj
Certifies that this is the approved version of the following thesis:

Application of Boundary Element Methods (BEM) to Internal Propulsion Systems; Application to Water-jets and Inducers

APPROVED BY

SUPERVISING COMMITTEE:

Spyridon A. Kinnas, Supervisor

Venkat Raman

Application of Boundary Element Methods (BEM) to Internal Propulsion Systems; Application to Water-jets and Inducers

by

Alokraj Valsaraj, B.E.

THESIS

Presented to the Faculty of the Graduate School of
The University of Texas at Austin
in Partial Fulfillment
of the Requirements
for the Degree of

MASTER OF SCIENCE IN ENGINEERING

THE UNIVERSITY OF TEXAS AT AUSTIN
August 2013

Dedicated to my loving parents P.Lathika and R.Valsaraj and my two brothers Amith and Varun.

Acknowledgments

I wish to thank my advisor Prof. Spyridon A. Kinnas for his continued guidance and support throughout my two years at UT Austin. I would also like to thank my reader Prof. Venkat Raman for taking the time to go through my thesis.

I also wish to thank my friends in the Ocean Engineering Group especially Ye Tian, Jay Purohit, David Menendez Aran, Chan-Hoo Jeon and Shu-Hao Chang who made my research fun and interesting.

Finally I would like to express my gratitude to my parents P.Lathika and R.Valsaraj and my two brothers Varun and Amith for their constant encouragement and support in all aspects of my life.

This work was supported by the U.S. Office of Naval Research (Contract N00014-10-1-0931) and members of the Phase VI of the Consortium on Cavitation Performance of High Speed Propulsors: American Bureau of Shipping, Kawasaki Heavy Industry Ltd., Rolls-Royce Marine AB, Rolls-Royce Marine AS, SSPA AB, Andritz Hydro GmbH, Wärtsilä Netherlands B.V., Wärtsilä Norway AS, Wärtsilä Lips Defense S.A.S. and Wärtsilä CME Zhenjiang Propeller Co. Ltd.

Application of Boundary Element Methods (BEM) to Internal Propulsion Systems; Application to Water-jets and Inducers

Alokraj Valsaraj, M.S.E.
The University of Texas at Austin, 2013

Supervisor: Spyridon A. Kinnas

A panel method derived from inviscid irrotational flow theory and utilizing hyperboloid panels is developed and applied to the simulation of steady fully wetted flows inside water-jet pumps and rocket engine inducers. The source and dipole influence coefficients of the hyperboloid panels are computed using Gauss quadrature.

The present method solves the boundary value problem subject to a uniform inflow directly by discretizing the blade, casing/shroud and hub geometries with panels. The Green's integral equation and the influence coefficients for the water-jet/inducer problem are defined and solved by allocating constant strength sources and dipoles on the blade, hub and casing surfaces and constant strength dipoles on the shed wake sheets from the rotor/ stator blades. The rotor- stator interaction is accomplished using an iterative procedure which considers the effect between the rotor and the stator, via circumferentially averaged induced velocities.

Finally, the hydrodynamic performance predictions for the water-jet pump and the inducer from the present method are validated against existing experimental data and numerical results from Reynolds Averaged Navier-Stokes (RANS) solvers .

Table of Contents

List of Figures

Nomenclature

Latin Symbols

C_f	skin-friction coefficient $C_f = \tau_{wall}/(0.5\rho U^2)$
C_p	pressure coefficient, $C_p = (p - p_o)/(0.5\rho n^2 D^2)$
D	propeller diameter, $D = 2R$
f_{max}/C	maximum camber to chord ratio
F_{nD}	Froude number based on V_A, $F_{nD} = V_A/\sqrt{gD}$
F_r	Froude number based on n, $F_r = n^2 D/g$
g	gravitational acceleration
G	Green's function
h_{gap}	gap size
J	advance ratio based on V_s, $J = V_s/(nD)$
K_Q	torque coefficient, $K_Q = Q/(\rho n^2 D^5)$
K_T	thrust coefficient, $K_T = T/(\rho n^2 D^4)$
n	propeller rotational frequency (rps)
p	pressure
p_o	pressure far upstream
p_v	vapor pressure of the fluid
P	pitch angle

$\boldsymbol{q}$	total velocity
Q	torque
$\boldsymbol{U}_{in}$	local inflow velocity (in the propeller fixed system)
$\boldsymbol{u}$	Perturbation velocity
R	propeller radius
Re	Reynolds number
S_R	rotor surface
S_{RW}	rotor wake surface
S_{HC}	hub and casing surfaces
S_S	stator surface
S_{SW}	stator wake surface
T	thrust

t_{max}/C	maximum thickness to chord ratio
τ_{wall}	wall shear stress
V_A	advance speed of propeller
u_τ	wall shear velocity, $u_\tau = \sqrt{\tau_{wall}/\rho}$
X, Y, Z	propeller fixed coordinates
X_S, Y_S, Z_S	ship fixed coordinates
y^+	non-dimensional wall distance, $y^+ = \frac{u_\tau y}{\nu}$

Greek Symbols

α	angle of attack
Γ	circulation
Δt	time step size
ν	kinematic viscosity of water
ϕ	perturbation potential
Φ	total potential
$\Delta\phi_{TE}$	potential jump at the trailing edge of the blade
$\Delta\phi_W$	potential jump across the shed wake sheet of the blade
ρ	fluid density
σ_n	cavitation number based on n, $\sigma_n = (p_o - p_v)/(0.5\rho n^2 D^2)$
σ_v	cavitation number based on V_A, $\sigma_v = (p_o - p_v)/(0.5\rho V_A^2)$
ω	propeller angular velocity

Uppercase Abbreviations

2D	two dimensional
3D	three dimensional
BEM	Boundary Element Method
CPU	Central processing unit
ITTC	International Towing Tank Conference
MIT	Massachusetts Institute of Technology
NACA	National Advisory Committee for Aeronautics
ONR-AXWJ	Office of Naval Research Axial Water-jet
RANS	Reynolds-Averaged Navier Stokes
SIMPLEC	Semi-Implicit Method for Pressure Linked Equations-Consistent scheme
VLM	Vortex-Lattice Method

Computer Program Names

FLUENT	A commercial RANS solver
PROPCAV	A cavitating propeller potential flow solver based on BEM
XFOIL	A 2D integral boundary layer analysis code

Chapter 1

Introduction

1.1 Introduction

A water-jet is a marine propulsion system that produces a jet of rapid water behind the ship for high-speed propulsion. The first working water-jet system was developed by Secondo Campini in Venice in 1931. Bill Hamilton, a New Zealand engineer built the first commercial water-jet propulsion system in 1954.

Initially water-jets were limited to high speed pleasure boats such as jet skis and jet boats. However the increasing demand for high-speed ships in recent years has led to the adoption of water-jet propulsion systems for commercial and naval vessels. Ships fitted with water-jet propulsion systems can achieve speeds up to 40 knots, even with a conventional hull. Luxury high speed motor yachts have achieved speeds above 65 knots, which is about 120 km/h. Figure 1.1 shows a marine vessel employing water-jet propulsion.

The nonexistence of appurtenances such as shafts, ducts and rudders below the waterline reduces the ship resistance and makes water-jets the chosen method for shallow water maneuvering. The damages from sizable debris to the propeller can be reduced inside the water-jet propulsion system. The

Figure 1.1: A high-speed police vessel utilizing water-jet propulsion (source: http://www.hamjet.co.nz/model_range).

occurrence of cavitation can also be reduced at lower ship speeds as compared to the open propeller. However cavitation can still occur at higher ship speeds and lead to thrust breakdown. The complicated geometry of the water-jet propulsion system, the inescapable cavitation due to pressure drops at high ship speeds and the innate unsteadiness of the rotor-stator interaction culminates in making the research and study of viscous flows in water-jet systems difficult. Figures 1.2 and 1.3 show the geometry configuration of a typical water-jet propulsion system.

1.2 Literature Review

Several numerical and experimental approaches have been developed and applied to analyse the water-jet propulsion system over the past two decades. An extensive study of the problems confronted in designing and

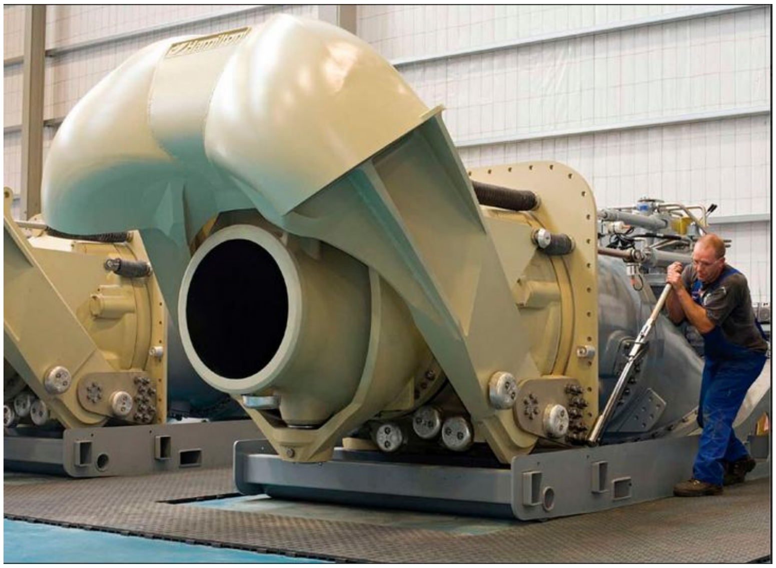

Figure 1.2: A water-jet propulsion system utilized for high-speed vessels (source: http://www.hamjet.co.nz/model_range) .

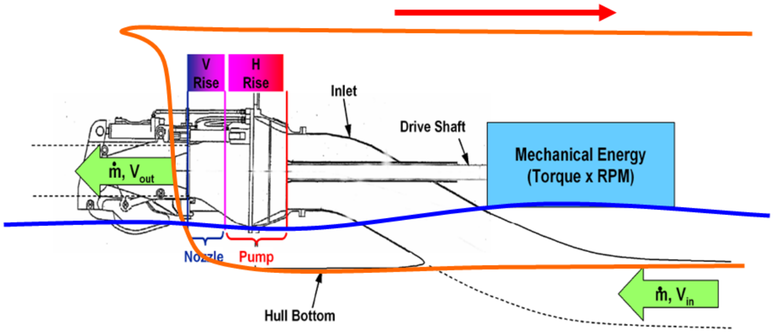

Figure 1.3: Schematic sketch of a water-jet propulsion system (from Chang, 2012).

calculating the hydrodynamic parameters of water-jet propulsion systems was carried out by Kerwin (2006). The International Towing Tank Conference paper (2008) presents a meticulous analysis and characterization of state of the art water-jet propulsion systems. Reynolds Averaged Navier-Stokes (RANS) schemes have been utilized with growing success for the analysis of internal flows in water-jet propulsion systems. Kim et al. (2002) used an in-house RANS code to compute a full water-jet system (inlet duct, rotor, stator and outlet nozzle) for a tracked vehicle. The authors used the code to look at some differences between two pump systems and to propose design changes to optimize the flow through the system. A RANS scheme employing a shifting, non-orthogonal grid was utilized by Chun et al. (2002) to study the rotor-stator interaction . The rotor was analyzed in an unsteady manner and the effect of the stator was considered in a circumferentially averaged manner. Brewton et al. (2006) employed a RANS scheme with the mixing plane model and analyzed the rotor-stator interaction in a water-jet propulsion system in a time-averaged manner. A RANS scheme with multiphase modeling ability was employed by Lindau et al. (2009; 2011). The authors utilized a power iteration algorithm to analyze a water-jet propulsion system at different flow coefficients and predict the thrust/torque breakdown due to cavitation.

The design and calculation of hydrodynamic performance parameters of water-jet propulsion systems have also been carried out using a transitional approach which couples a potential flow scheme with a RANS scheme. A vortex lattice scheme combined with either an Euler equation solver or a RANS scheme was utilized by Kerwin et al. (1997) and Taylor et al. (1998) to consider the impact of the hull and to study the entire flow in a water-jet propulsion system. A potential flow panel method was employed by Kinnas, Chang et al.(2007, 2010, 2012) to calculate the hydrodynamic performance parameters of a water-jet propulsion system. The rotor- stator interaction was accomplished using an iterative procedure which considers the effect of circumferentially averaged induced potentials between the rotor and the stator. Sun and Kinnas et al. (2006) and Kinnas et al. (2007) have analyzed the effects of viscous flow through ducted propellers and the ONR-AXWJ1 water-jet propulsion system by coupling the potential flow panel method with the boundary layer method XFOIL (Drela, 1989). This numerical approach is capable of capturing the repercussions of the boundary layer on the blade cavities.

1.3 Objectives

- The objective of this thesis is to refine and enhance a potential flow solver PROPCAV, based on the panel method by Kinnas and Fine (1993), and to analyze the steady fully-wetted performance of water-jet propulsion systems.

- The present panel method will be used to evaluate the hydrodynamic performance characteristics of the water-jet propulsion system and the results will be compared with RANS calculations.

- The present panel method will utilize a numerical scheme to evaluate the dipole and source influence coefficients of non-planar hyperboloid surface panels more accurately.

- The numerical panel method will also be extended to analyze the performance of an inducer as further demonstration of its applicability.

1.4 Organization

This thesis is organized into five chapters.

Chapter 1 contains the literature review, the objectives and the organization of this study.

Chapter 2 explains the methodology, governing equations and boundary conditions utilized in the present numerical method.

Chapter 3 describes the application of the numerical panel method for the analysis and hydrodynamic performance prediction of water-jet propulsion systems.

Chapter 4 describes the extension of the numerical panel method to study rocket engine inducers.

Chapter 5 presents the conclusions and the recommendations for future work.

Chapter 2

Methodology

A numerical panel method is refined and enhanced to analyze water-jet propulsion systems. This chapter describes the governing equations, the numerical method and the boundary conditions involved in solving inviscid wetted flows inside a water-jet propulsion system.

2.1 Governing Equations

The typical configuration of a water-jet propulsion system along with its coordinate systems is shown in Figure 2.1. The ship fixed coordinate system is denoted by (X_s, Y_s, Z_s) and (X, Y, Z) represents the propeller fixed coordinate system. The inflow $\vec{U}$ specified at the water-jet inlet is defined in a ship fixed coordinate system and is assumed to be uniform for steady problems.

The rotor blades rotate with a constant angular velocity vector $\vec{\omega}$. The stator blades do not rotate and are fixed with respect to the propeller coordinate system $\vec{X}$. Therefore the total inflow velocity $\vec{V}_{in}$ in the propeller fixed coordinate system can be expressed as $\vec{V}_{in} = \vec{U} + \vec{\omega} \times \vec{X}$ for the rotor and $\vec{V}_{in} = \vec{U}$ for the stator. The velocity field for an inviscid, irrotational and incompressible flow, in the rotating frame of reference, is expressed as

$$\vec{q_t}(x, y, z) = \vec{V}_{in}(x, y, z) + \nabla\phi(x, y, z) \tag{2.1}$$

where $\vec{q_t}(x, y, z)$ is the total velocity at any point inside the fluid domain, ϕ is the perturbation potential which satisfies the Laplace equation $\nabla^2\phi = 0$.

The perturbation potential $\phi(x, y, z)$ at any point on the rotor (S_R),stator (S_S), hub (S_H) and casing (S_C) surfaces has to satisfy the Green's third identity as given in equation 2.2.

$$\begin{aligned} 2\pi\phi = &\int_{S_R} \left[\phi_q \frac{\partial G(p;q)}{\partial n_q} - G(p;q)\frac{\partial \phi}{\partial n_q}\right] ds \\ &+ \int_{S_{R_W}} \triangle\phi_{R_W} \frac{\partial G(p;q)}{\partial n_q} ds \\ &+ \int_{S_S} \left[\phi_q \frac{\partial G(p;q)}{\partial n_q} - G(p;q)\frac{\partial \phi}{\partial n_q}\right] ds \\ &+ \int_{S_{S_W}} \triangle\phi_{S_W} \frac{\partial G(p;q)}{\partial n_q} ds \\ &+ \int_{S_{HC}} \left[\phi_q \frac{\partial G(p;q)}{\partial n_q} - G(p;q)\frac{\partial \phi}{\partial n_q}\right] ds \end{aligned} \tag{2.2}$$

where p and q correspond to the variable point and the field point respectively, $G(p : q) = \frac{1}{R(p;q)}$ is the Green function and $R(p;q)$ is the distance between the field point p and the variable point q,n indicates the normal direction pointing into the flow field, $\triangle\phi_{R_W}$ and $\triangle\phi_{S_W}$ are the potential jumps across the trailing wake sheets shed from the rotor and the stator blade trailing edge respectively.

The flow inside a water-jet propulsion system is simulated through an iterative procedure which solves the rotor problem and the stator problem

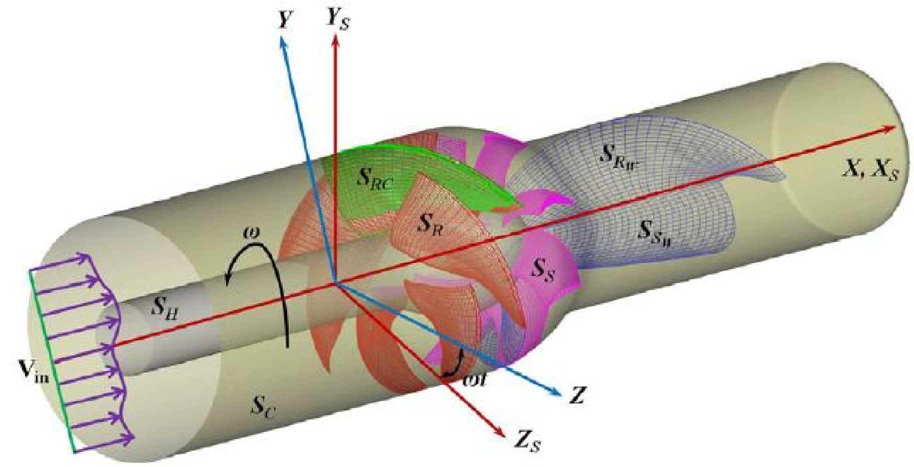

Figure 2.1: Coordinate systems utilized for the analysis of a water-jet propulsion system (Kinnas et al. 2012)

separately and accounts for the rotor-stator interaction by considering the circumferentially averaged effects of each component on the other. A fully unsteady simulation as given in Tian (2013) needs to be performed in order to totally capture the interaction between the rotor and the stator. The computational resources required for such a simulation is exceedingly expensive.

The rotor-stator interaction is carried out via induced velocities in the present method. Hence the numerical method is known as the induced velocity method. In addition, the rotor is solved with respect to the rotating coordinate system and the stator is solved with respect to the ship fixed coordinate system. Figure 2.2 is the diagrammatic outline of the rotor and stator problem, the rotor only problem, and the stator only problem respectively. More details on the induced velocity method for the rotor-stator interaction can be found in Chang (2012).

2.2 Numerical Method

The integral equations for the rotor and stator problems and the calculation of the circumferentially averaged induced velocities are presented in this section.

2.2.1 Rotor only problem

The integral equation for the rotor problem is given as

$$\begin{aligned}2\pi\phi = &\int_{S_R}\left[\phi_q\frac{\partial G(p;q)}{\partial n_q} - G(p;q)\frac{\partial\phi}{\partial n_q}\right]ds\\ &+\int_{S_{R_W}}\triangle\phi_{R_W}\frac{\partial G(p;q)}{\partial n_q}ds\\ &+\int_{S_{HC}}\left[\phi_q\frac{\partial G(p;q)}{\partial n_q} - G(p;q)\frac{\partial\phi}{\partial n_q}\right]ds\end{aligned} \tag{2.3}$$

where the source strength $\partial\phi/\partial n$ is modified as

$$\frac{\partial\phi}{\partial n} = -(\vec{V}_{in} + \vec{u}_{RS}).\vec{n} \tag{2.4}$$

where $\vec{u}_{RS}$ is the circumferentially averaged velocities on the rotor, hub and casing surfaces induced by the stator which are evaluated from the following integral equation

$$\begin{aligned}4\pi\vec{u}_{RS} = &\int_{S_S}\left[\phi_q\nabla\frac{\partial G(p;q)}{\partial n_q} - \nabla G(p;q)\frac{\partial\phi}{\partial n_q}\right]ds\\ &+\int_{S_{S_W}}\triangle\phi_{S_W}\nabla\frac{\partial G(p;q)}{\partial n_q}ds\end{aligned} \tag{2.5}$$

More information on calculating the induced potentials and velocities can be obtained from Newman (1986).

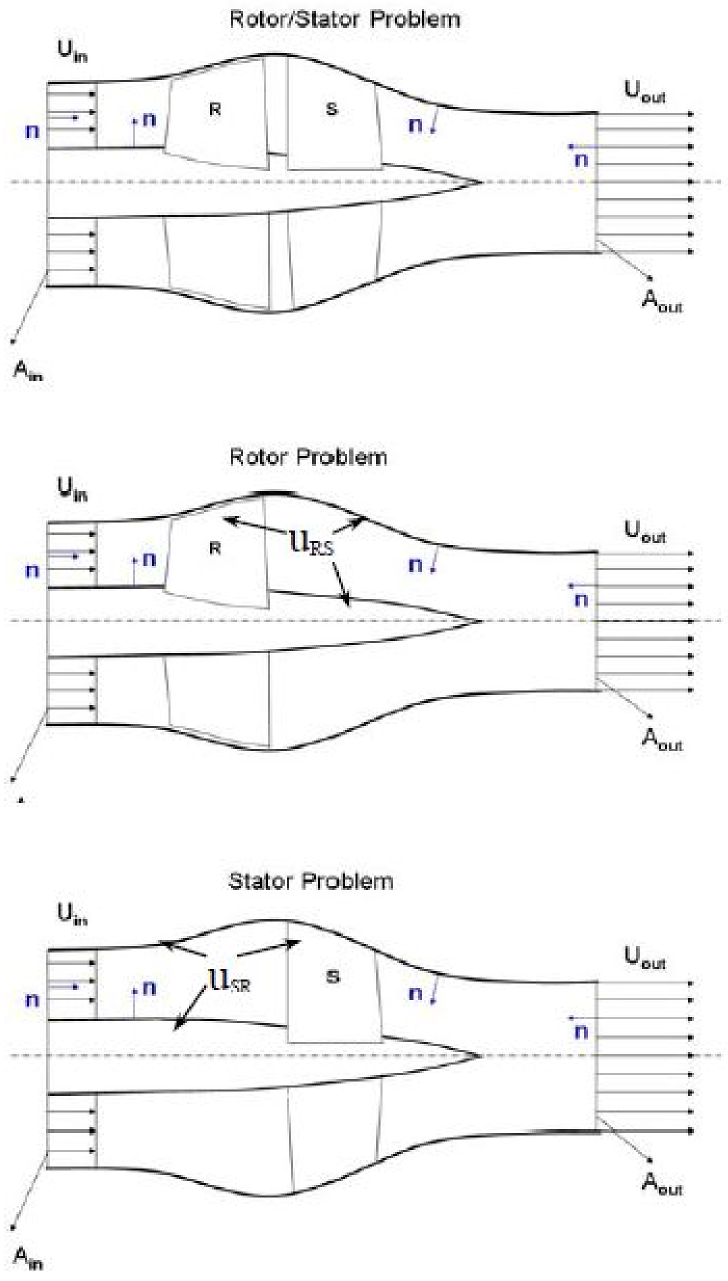
Rotor/Stator Problem

Rotor Problem

Stator Problem

Figure 2.2: Diagrammatic outline of the rotor and stator problem, the rotor only problem and the stator only problem. (from Kinnas et al., 2007).

2.2.2 Stator only problem

The integral equation for the stator problem is given as

$$\begin{aligned}2\pi\phi = &\int_{S_S}\left[\phi_q\frac{\partial G(p;q)}{\partial n_q} - G(p;q)\frac{\partial \phi}{\partial n_q}\right]ds \\ &+ \int_{S_{S_W}} \triangle\phi_{R_W}\frac{\partial G(p;q)}{\partial n_q}ds \\ &+ \int_{S_{HC}}\left[\phi_q\frac{\partial G(p;q)}{\partial n_q} - G(p;q)\frac{\partial \phi}{\partial n_q}\right]ds\end{aligned} \tag{2.6}$$

where the source strength $\partial\phi/\partial n$ is modified as

$$\frac{\partial\phi}{\partial n} = -(\vec{V}_{in} + \vec{u}_{SR}).\vec{n} \tag{2.7}$$

where $\vec{u}_{SR}$ is the circumferentially averaged velocities on the stator, hub and casing surfaces induced by the stator which are evaluated from the following integral equation

$$\begin{aligned}4\pi\vec{u}_{SR} = &\int_{S_R}\left[\phi_q\nabla\frac{\partial G(p;q)}{\partial n_q} - \nabla G(p;q)\frac{\partial \phi}{\partial n_q}\right]ds \\ &+ \int_{S_{R_W}} \triangle\phi_{S_W}\nabla\frac{\partial G(p;q)}{\partial n_q}ds\end{aligned} \tag{2.8}$$

2.3 Boundary conditions

The following boundary conditions need to be satisfied for analyzing the water-jet system. The kinematic boundary condition on the rotor, stator, hub and casing surfaces requires that the flow must be tangent to the body surfaces.

$$\frac{\partial\phi}{\partial n} = -\vec{V}_{in}.\vec{n} \tag{2.9}$$

The Kutta condition ensures that the velocities at the trailing edge of the blade are finite. An iterative pressure Kutta condition is applied to ensure that the pressures on the pressure side and suction side of the blade trailing edge are equal. Further details are given in Kinnas and Hsin (1992).

The flow field is assumed to equal the inflow velocity at the inlet of the water-jet system.

$$\left.\frac{\partial \phi}{\partial n}\right|_{inflow} = 0 \tag{2.10}$$

It should be noted that the inlet panels of the water-jet are removed and the perturbation potentials are set to be zero on those panels to obtain an unique solution of the internal boundary value problem.

The conservation of mass law must be fulfilled at the water-jet outlet. Hence we obtain

$$V_{in} \cdot A_{in} = V_{out} \cdot A_{out} \tag{2.11}$$

where V_{in} is the inlet velocity, A_{in} and A_{out} are the water-jet inflow and outflow surface areas respectively.

2.4 Numerical evaluation of influence coefficients

This section describes the evaluation of dipole and source influence coefficents using numerical integration for hyperboloid panels. The numerical integration is accomplished using Gauss quadrature.

2.4.1 Gauss quadrature

The Green's integral equation 2.2 can be written in the following discretized form on all the panels, with the Green function $G(p:q) = \frac{1}{R(p;q)}$ and $\frac{\partial\phi}{\partial n_q} = -\vec{V}_{in}.\vec{n}_q$,

$$\sum_k A_{lk}\phi_k = \sum_k (-\vec{V}_{in}.\vec{n}_k)B_{lk} \tag{2.12}$$

The dipole influence coefficient A_{lk} is given as

$$A_{lk} = \int\int_{S_k} \vec{n}_k \cdot \nabla(\frac{1}{r_{lk}})ds_k \tag{2.13}$$

and the source influence coefficent B_{lk} is given as

$$B_{lk} = \int\int_{S_k} \frac{1}{r_{lk}}ds_k \tag{2.14}$$

where $\vec{n}_k$ represents the normal vector, r_{lk} represents the distance to the control point and ds_k represents the elemental surface area.

The discretized form of the dipole (A_{lk}) and source (B_{lk}) influence coefficients associated with a panel is

$$A = \sum_{i=1}^{n}\sum_{j=1}^{n} \vec{n}_{ij} \cdot \nabla(\frac{1}{r_{ij}})w_{ij}\Delta s \tag{2.15}$$

$$B = \sum_{i=1}^{n}\sum_{j=1}^{n} \frac{1}{r_{ij}}w_{ij}\Delta s \tag{2.16}$$

where (i, j) represents the Gaussian point on the panel, $\vec{n}_{ij}$ represents the normal vector, n represents the number of Gaussian points on the panel and r_{ij} represents the distance to the control point as shown in Figure 2.3. Here

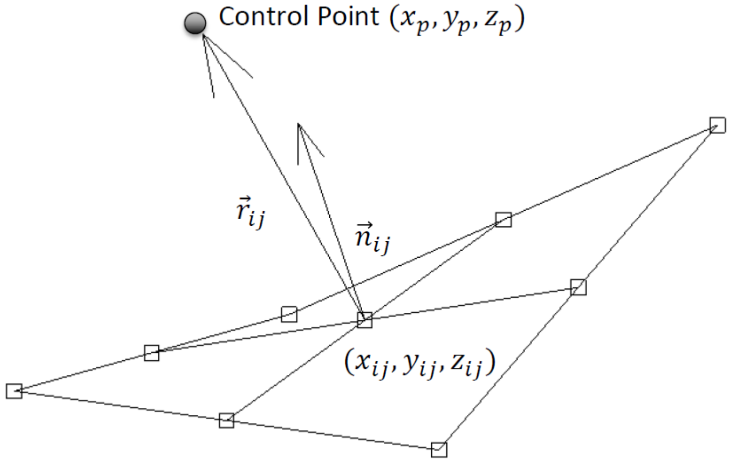

Figure 2.3: A panel discretized with Gaussian points to evaluate the influence coefficients numerically. The interior of the panel is discretized with $n = 3$ Gaussian points.

w_{ij} represents the weight for each Gaussian point and the surface area

$\Delta s = \Delta x \Delta y |J|$ where J is the Jacobian.

The present panel method uses $n = 8$ Gaussian points to discretize the panel. We have also tried $n = 4$ and $n = 16$ Gaussian points to discretize the panel. The time taken to complete 10^4 calculations for a panel discretized with $n = 4$, $n = 8$ and $n = 16$ Gaussian points are $7s$, $10s$ and $18s$ respectively. Hence we decided to select $n = 8$ Gaussian points to provide a balance between accuracy and speedy computation.

2.4.2 Non-planar quadrilateral

In order to validate the Gauss quadrature scheme, we use it to calculate the dipole and source influence coefficients of a non-planar quadrilateral as shown in Figure 2.4. The control point is moved along the z axis.

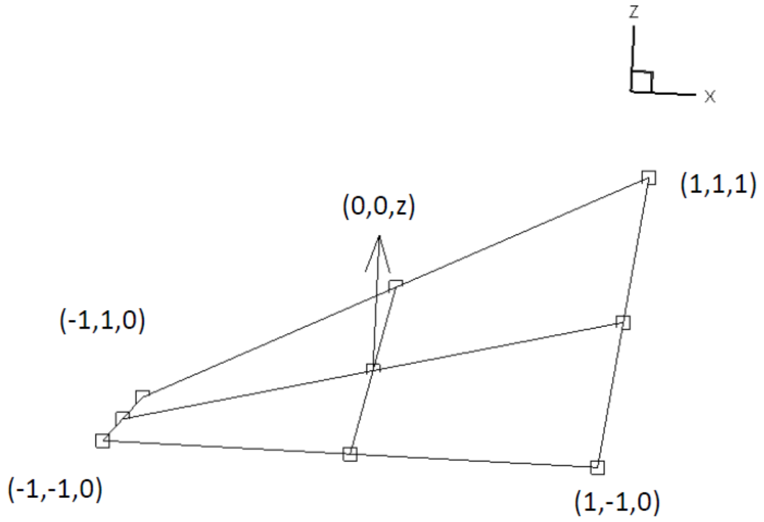

Figure 2.4: The non-planar quadrilateral considered for evaluating the influence coefficients. The control point is moved along the z axis.

The relative error in calculating the dipole and source influence coefficients are shown in Figures 2.5 and 2.6 respectively. The relative error is defined as

$$relative\, error = (\frac{|v_{numerical} - v_{exact}|}{|v_{exact}|}) \tag{2.17}$$

The exact value is obtained using MATLAB to compute the integrals.

It is observed that the relative error in evaluating the dipole influence coefficient by Gauss quadrature scheme increases rapidly as the control point is moved very close to the panel. This is because the numerical scheme in its present form cannot resolve the singularity in A as $r_{ij} \to 0$. This error is mitigated by evaluating the dipole influence coefficients of a hyperboloid

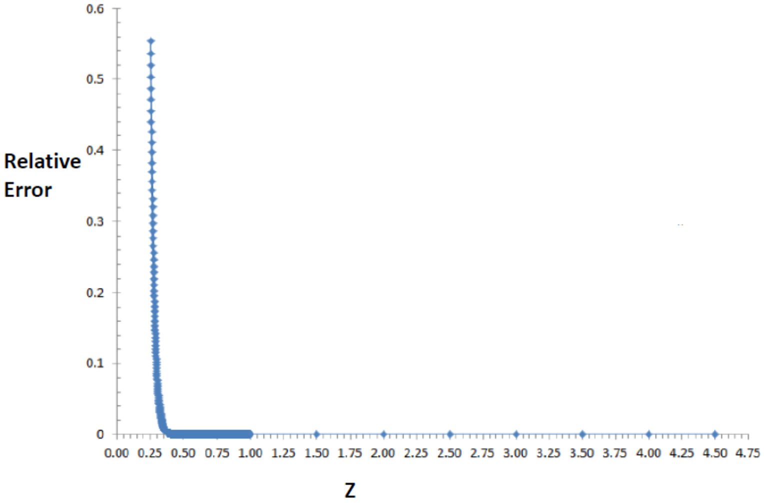

Figure 2.5: Relative error in calculating the dipole influence coefficient of the non-planar quadrilateral shown in Figure 2.4. The control point is moved along the z axis.

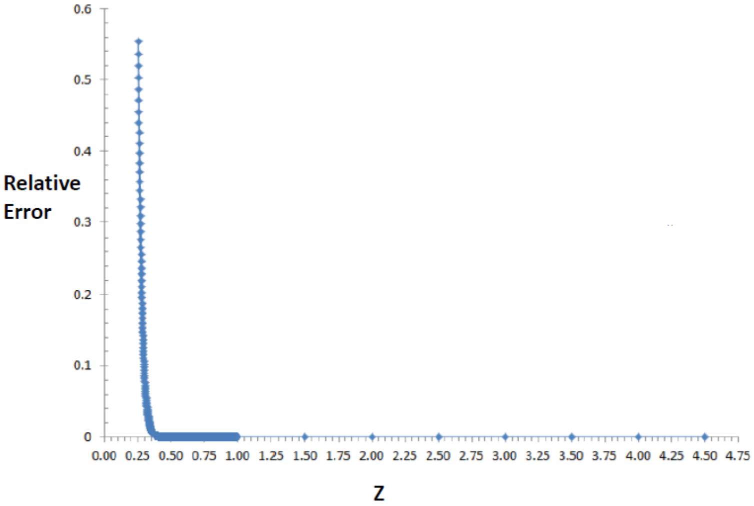

Figure 2.6: Relative error in calculating the source influence coefficient of the non-planar quadrilateral shown in Figure 2.4. The control point is moved along the z axis.

panel using the approach developed by Morino, Chen and Suciu (1975). However this scheme is valid only for control points very close to the panel. Henceforth for the calculation of the dipole influence coefficients we will use the Morino formula for control points very close to the panel (like self-influence coefficients) and Gauss quadrature for control points farther away.

2.4.3 Casing only problem

After using the Gauss quadrature numerical scheme to analyze a single non-planar panel, we move on to a simplified case, considering the casing only problem of a water-jet propulsion system. The casing selected was the casing of a water-jet propulsion system as shown in Figure 2.8.

The paneling on the casing of the water-jet system follows the pitch angle (P) of the rotor blade. The pitch angle of a rotor blade is the angle between the chord line and a reference plane determined by the rotor hub or the plane of rotation as shown in Figure 2.7. For low pitch rotor blades we have highly skewed panels on the casing. The planar method used to evaluate the influence coefficients is RPAN (Newman 1986), which handles non-planar panels as planar panels resulting from the projection of the non-planar panel on the midpoint plane. This method requires a large number of panels to properly evaluate the dipole and source influence coefficients for low pitch cases. However using hyperboloid panels and the non-planar numerical method allows us to significantly reduce the number of panels used to discretize the surface of the casing.

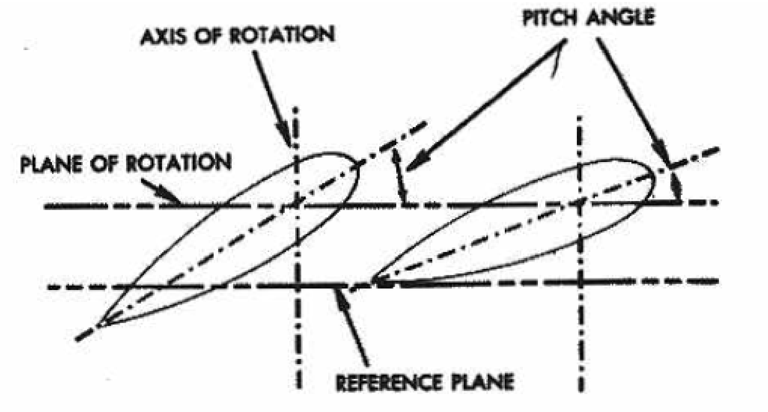

Figure 2.7: The pitch angle of a rotor blade is the angle between the chord line and a reference plane (source: http://www.allstar.fiu.edu/aero/flight63.htm).

In the study, the pitch angle considered is 80^o as shown in Figure 2.8. The total number of panels used to discretize the casing is 4000. The number of axial elements is 240 and the number of circumferential elements is 40 on the casing. The results for $P = 80^o$ case given in Figure 2.9 are also compared with the results for $P = 0^o$ case given in Figure 2.10 where both the planar and non-planar methods work very well. We observe that the non-planar method works admirably well for $P = 80^o$ case while the planar method fails for the same case.

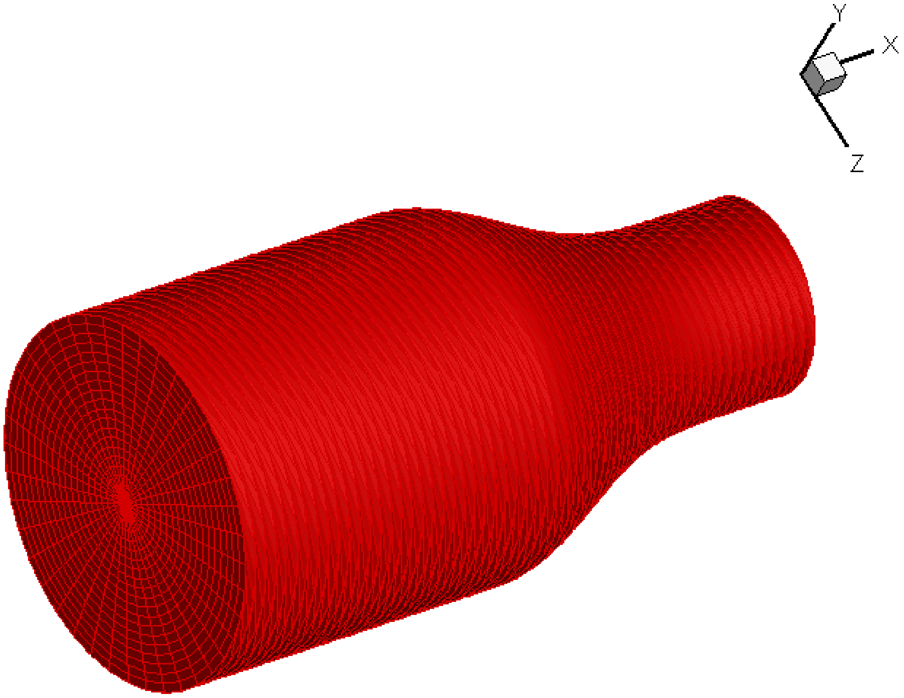

Figure 2.8: Paneling on the water-jet casing for $P = 80^o$ case. The total number of panels used to discretize the casing is 4000.The number of axial elements is 240 and the number of circumferential elements is 40 on the casing.

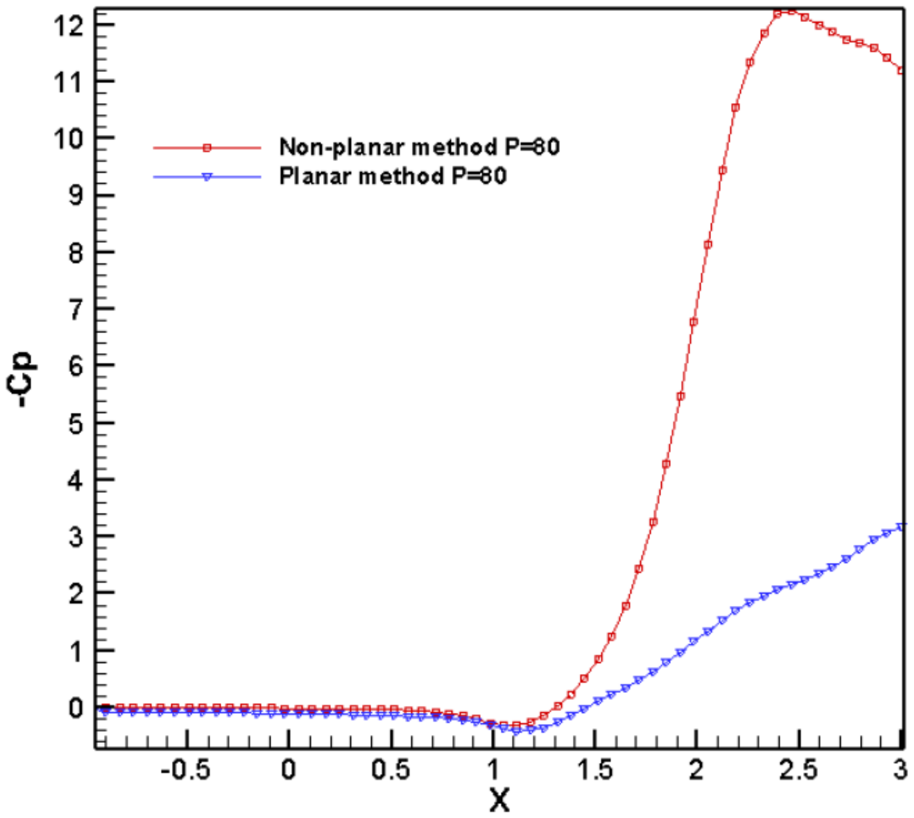

Figure 2.9: Pressure distribution on the casing for $P = 80^o$ case . The total number of panels used to discretize the casing is 4000.The number of axial elements is 240 and the number of circumferential elements is 40 on the casing.

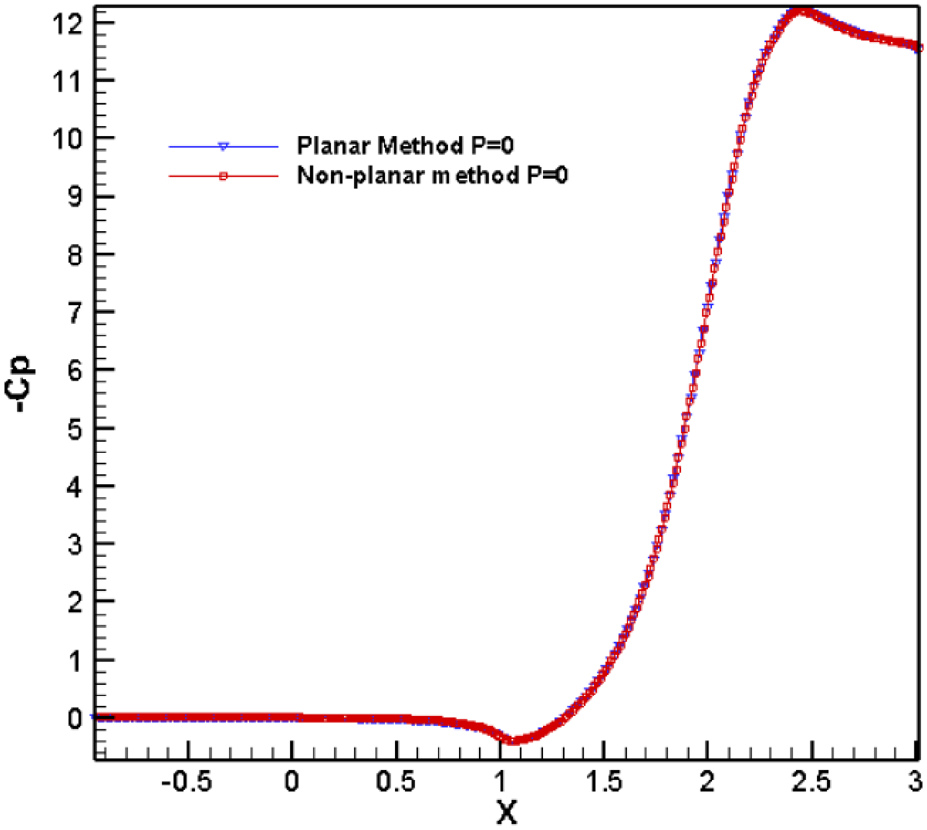

Figure 2.10: Pressure distribution on the casing for $P = 0^o$ case. The total number of panels used to discretize the casing is 4000.The number of axial elements is 240 and the number of circumferential elements is 40 on the casing.

Chapter 3

Numerical Analysis of Water-jets

This chapter presents the numerical analysis of axial flow water-jet pumps using the present panel method. The present study considers water-jets subject to a uniform inflow and only the steady simulations are considered here. The interaction between the rotor and the stator is carried out by applying the induced velocity method. The design advance ratio is 1.19 and the rotational frequency is 1400 rpm for the fully wetted condition. The numerical results from the present panel method are compared with Reynolds Averaged Navier-Stokes (RANS) calculations using FLUENT.

3.1 Nondimensional Coefficients

The nondimensional coefficients utilized in this thesis are explained below. The circulation Γ is given from Kinnas (2012)

$$\Gamma = \frac{\Delta\phi}{2\pi R\sqrt{U_{in}^2 + (0.7n\pi D)^2}} \tag{3.1}$$

where $\triangle\phi$ indicates the potential jump at trailing edge of the rotor blade in the present method. The advance ratio J_s and the Reynolds number Re are also given as:

$$J_s = \frac{U_{in}}{nD}, \quad Re = \frac{U_{in}R}{\nu} \tag{3.2}$$

where U_{in} is the flow velocity at the inlet boundary, R represents the radius of the rotor and νdenotes the kinematic viscosity.The pressure coefficient C_p used in the present method is defined as follows

$$C_p = \frac{p - p_o}{0.5\rho n^2 D^2} \tag{3.3}$$

where p_o is the far upstream pressure on the shaft axis.

3.2 Rotor only Case

Two different cases are considered in this section for the rotor only analysis. The only difference between these two cases is in the geometry of the casing. First we will present the results obtained by analyzing the water-jet rotor system with a cylindrical casing. Then we will move on to the more realistic case of the Office of Naval Research Axial Water-jet (ONR-AXWJ2) rotor pump.

3.2.1 Rotor with cylindrical casing

The paneled geometry of the rotor analysed with the present numerical method is shown in Figure 3.1. The rotor blade has the NACA-16 thickness form and a sharp trailing edge. The present method takes 10 minutes for a fully-wetted analysis by using 120 × 40 panels on the blade, 90 × 20 panels on the hub and 200 × 20 panels on the casing. The first number in the legend 120 × 40 denotes the number of panels in the chord-wise or axial direction and the second number denotes the number of elements in the span-wise

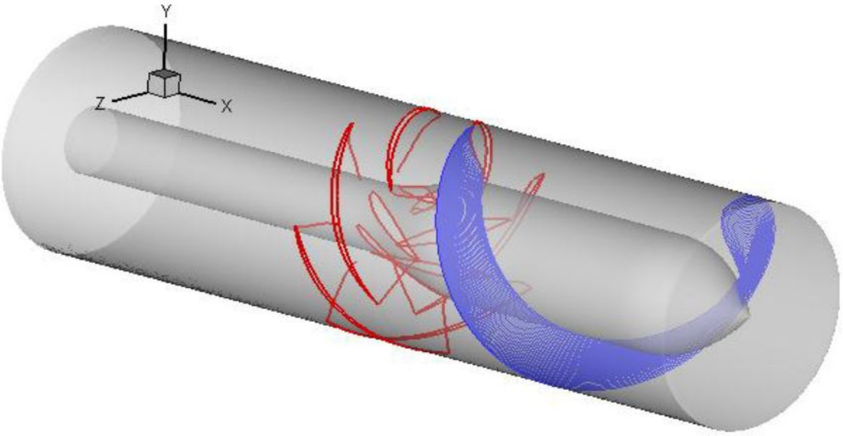

Figure 3.1: The paneled geometry of the rotor only water-jet system with a 6 bladed rotor viewed from downstream. There are 120 × 40 panels on the blade, 90 × 20 panels on the hub and 200 × 20 panels on the casing. There is no gap between the rotor blade and the casing. This is the rotor only system with the cylindrical casing as well as the NACA-16 thickness rotor blade and a sharp trailing edge.

direction on the blade or the circumferential direction between two blades. There is no gap between the casing and the blade in the simulation performed using the panel method.

The results from the present panel method including the circulation distribution on the rotor blade and the pressure distributions on the rotor sections and casing are compared with those from the Reynolds Averaged Navier-Stokes (RANS) solver FLUENT. A 3-D rotor only periodic mesh consisting of 5.94 million cells as shown in Figure 3.2 is used to perform the RANS simulation. Both inviscid and viscous simulations are performed using FLUENT. The SIMPLEC scheme is used for the pressure-velocity coupling in the simulation. There is no gap between the casing and the blade in the periodic mesh. The $k - \omega$ SST model is used for the viscous simulation. The moving wall boundary condition is used on the casing and the hub. The y^+ varies from 50 to 400 on the hub and from 40 to 180 on the casing. The simulations take about 8 hours by using 16 CPUs to complete 20,000 iterations on a cluster with 2.43 GHZ quad-core 64-bit Intel Xeon processors and 16 GB of RAM.

Figure 3.3 shows the circulation distributions on the rotor blade from the present panel method PROPCAV and the FLUENT inviscid run. Figures 3.4 to 3.6 show the pressure distributions on the rotor blade from the present panel method and FLUENT viscous and inviscid runs at different radii. The two $C_p(mean)$ curves presented in Figure 3.7 are obtained by circumferentially averaging pressures over all the strips on the casing surface from the 3-D FLUENT simulation and those from the present panel method. Figure 3.7 shows that the pressure rise on the casing surface from the present panel method and the viscous FLUENT simulation are in good agreement.

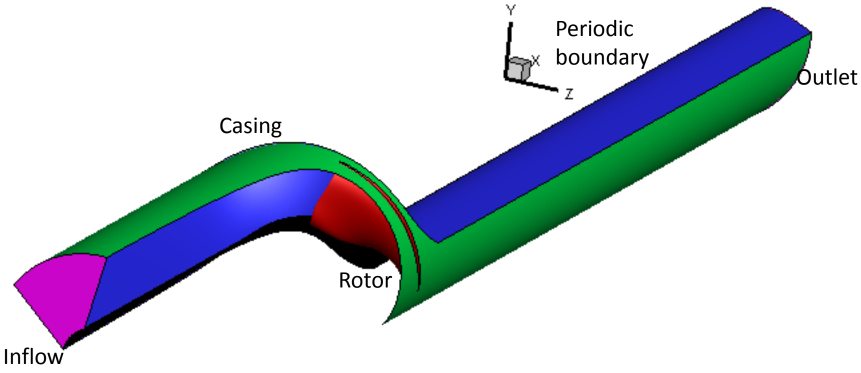

Figure 3.2: The 3D periodic mesh consisting of 5.94 million cells used for the RANS simulation. There is zero gap between the casing and the rotor blade. This is the rotor only system with the cylindrical casing as well as the NACA-16 thickness rotor blade and a sharp trailing edge.

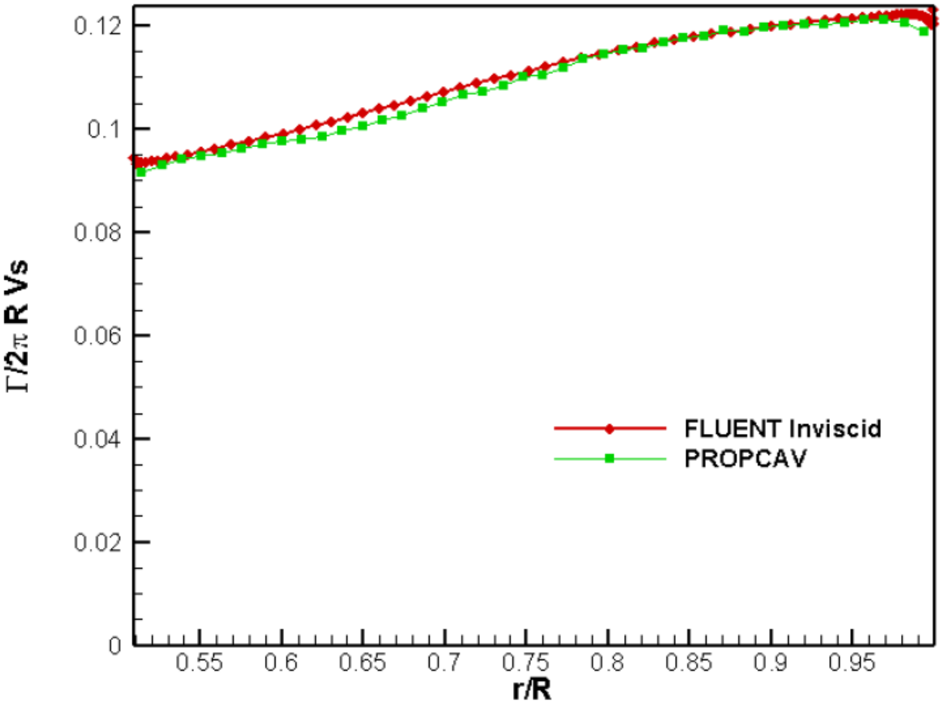

Figure 3.3: Comparison of circulation distributions on the rotor blade from the present panel method and FLUENT inviscid run at advance coefficient $J = 1.19$.There are 120×40 panels on the blade, 90×20 panels on the hub and 200×20 panels on the casing. The 3D periodic mesh has 5.94 million cells. This is the rotor only system with the cylindrical casing as well as the NACA-16 thickness rotor blade and a sharp trailing edge.

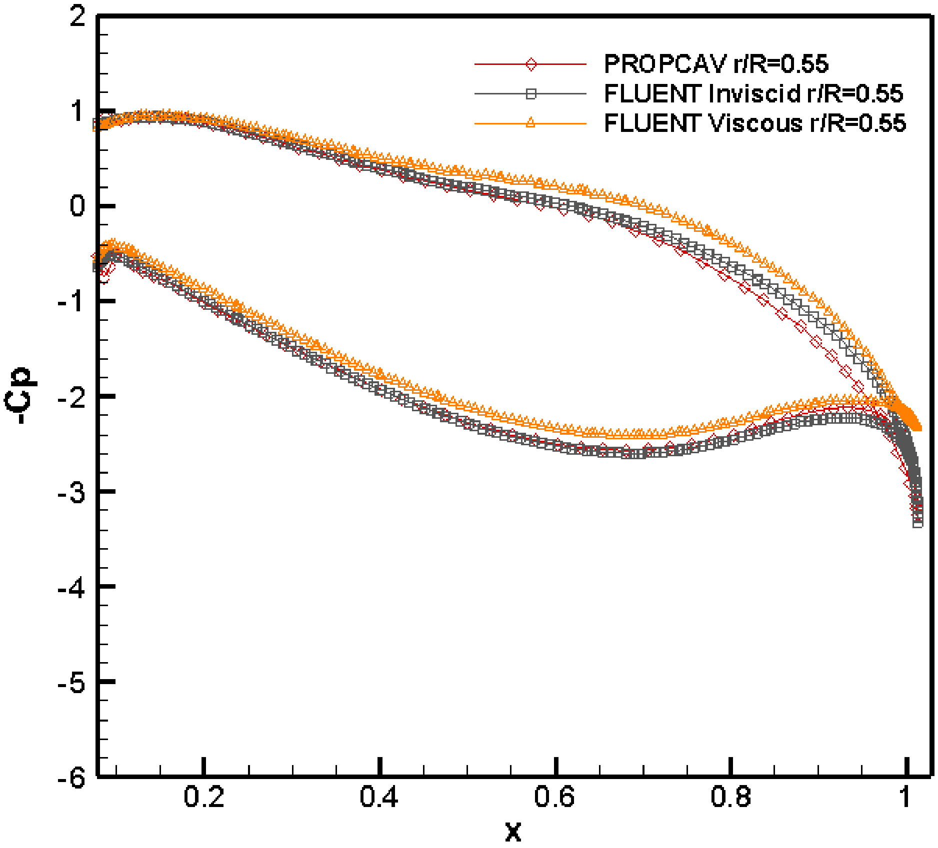

Figure 3.4: Comparison of pressure distributions on the rotor blade from the present panel method and FLUENT inviscid and viscous runs at advance coefficient $J = 1.19$ and radius of 0.55. There are 120×40 panels on the blade, 90×20 panels on the hub and 200×20 panels on the casing. The 3D periodic mesh has 5.94 million cells. This is the rotor only system with the cylindrical casing as well as the NACA-16 thickness rotor blade and a sharp trailing edge.

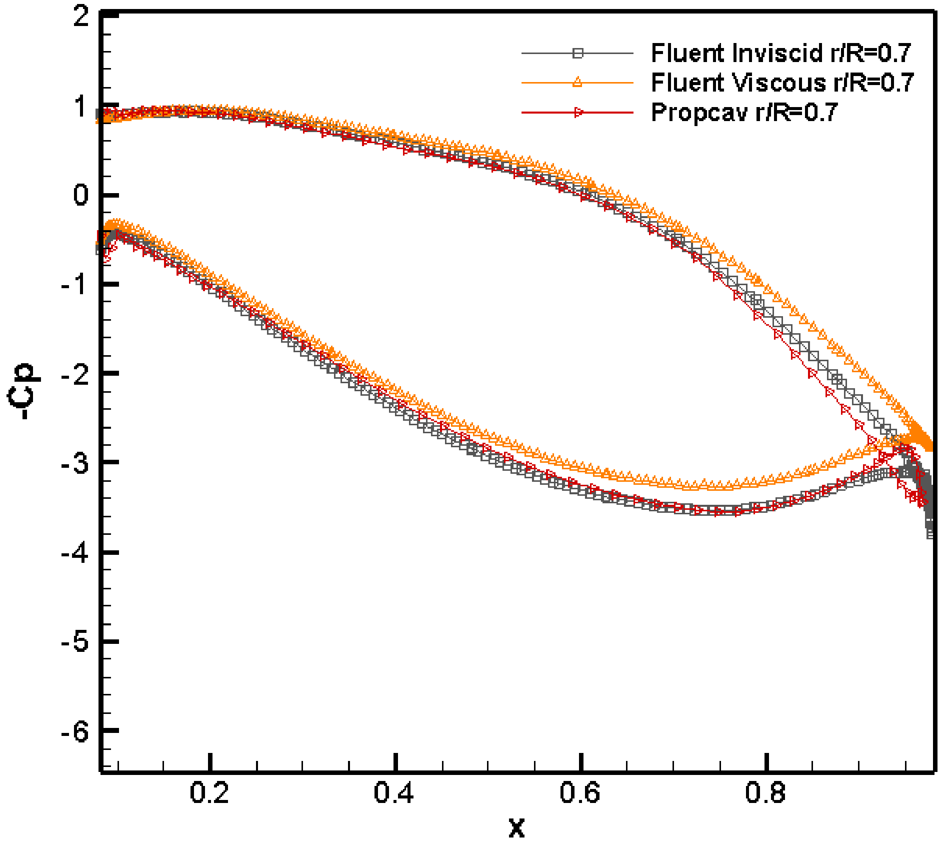

Figure 3.5: Comparison of pressure distributions on the rotor blade from the present panel method and FLUENT inviscid and viscous runs at advance coefficient $J = 1.19$ and radius of 0.70. There are 120×40 panels on the blade, 90×20 panels on the hub and 200×20 panels on the casing. The 3D periodic mesh has 5.94 million cells. This is the rotor only system with the cylindrical casing as well as the NACA-16 thickness rotor blade and a sharp trailing edge.

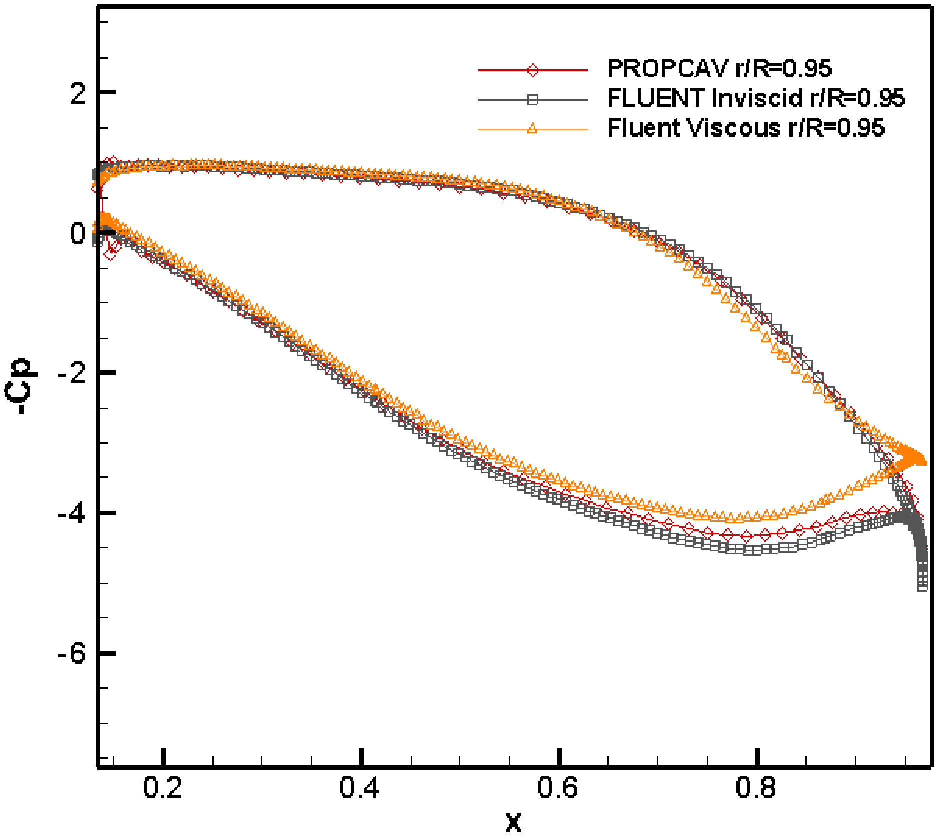

Figure 3.6: Comparison of pressure distributions on the rotor blade from the present panel method and FLUENT inviscid and viscous runs at advance coefficient $J = 1.19$ and radius of 0.95. There are 120×40 panels on the blade, 90×20 panels on the hub and 200×20 panels on the casing. The 3D periodic mesh has 5.94 million cells. This is the rotor only system with the cylindrical casing as well as the NACA-16 thickness rotor blade and a sharp trailing edge.

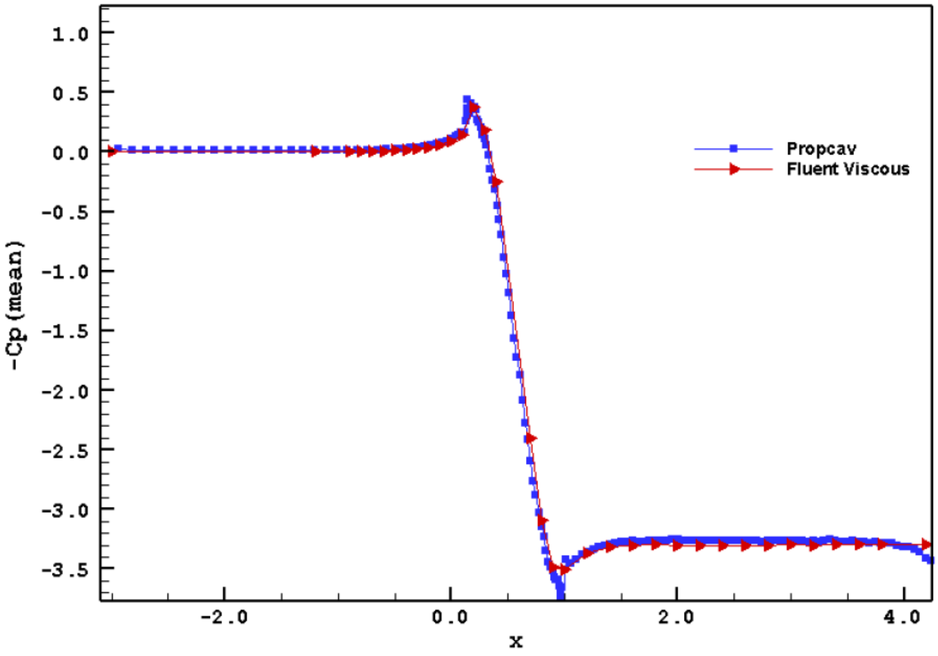

Figure 3.7: Comparison of circumferentially averaged pressure distributions on the casing surface from the present panel method and FLUENT viscous run at advance coefficient $J = 1.19$. There are 120×40 panels on the blade, 90×20 panels on the hub and 200×20 panels on the casing. The 3D periodic mesh has 5.94 million cells. This is the rotor only system with the cylindrical casing as well as the NACA-16 thickness rotor blade and a sharp trailing edge.

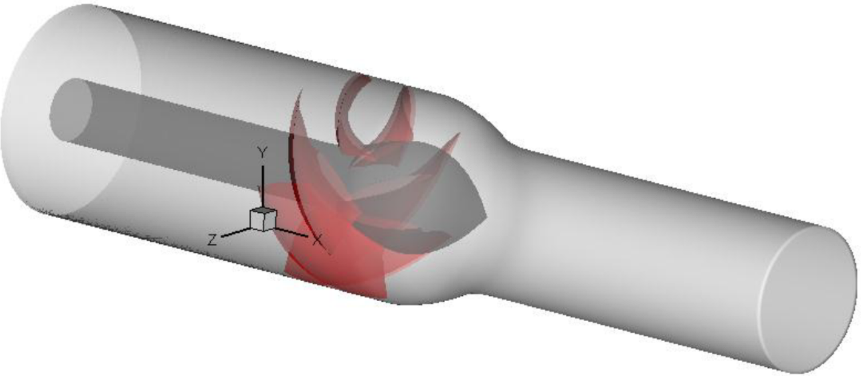

Figure 3.8: The paneled geometry of the ONR-AXWJ2 rotor only system with the 6 bladed rotor viewed from downstream. There are 120 × 40 panels on the blade, 90 × 20 panels on the hub and 160 × 20 panels on the casing. There is no gap between the casing and the blade. This is the ONR-AXWJ2 rotor only system with the NACA-16 thickness rotor blade and a sharp trailing edge.

3.2.2 ONR-AXWJ2 Rotor Case

The paneled geometry of the rotor analysed with the present numerical method is shown in Figure 3.8. The rotor blade has the NACA-16 thickness form and a sharp trailing edge. The present method takes 8 minutes for a fully-wetted analysis by using 120 × 40 panels on the blade, 90 × 20 panels on the hub and 160 × 20 panels on the casing. There is no gap between the casing and the blade in the simulation performed using the panel method.

The results from the present panel method including the pressure distributions on the rotor sections and the casing are compared with those from the Reynolds Averaged Navier-Stokes (RANS) solver FLUENT. A 3-D rotor only periodic mesh consisting of 2.3 million cells as shown in Figure 3.9 is used to perform the RANS simulation. We have only performed viscous simulations in FLUENT using the created mesh. The SIMPLEC scheme is used for the pressure-velocity coupling in the simulation. There is a gap of 0.33% between the casing and the blade in the periodic mesh. The $k-\omega$ SST model is used for the viscous simulation. The stationary wall boundary condition is used on the casing and the moving wall boundary condition on the hub. The y^+ varies from 50 to 420 on the hub and from 40 to 190 on the casing. There are 10 layers in the tip gap region of the mesh. The simulations take about 10 hours by using 16 CPUs to complete 20,000 iterations on a cluster with 2.43 GHZ quad-core 64-bit Intel Xeon processors and 16 GB of RAM.

Figure 3.10 shows the circulation distributions on the rotor blade from the present panel method. Figures 3.11 to 3.13 show the pressure distributions on the rotor blade from the present panel method and FLUENT viscous and inviscid runs at different radii.

The two $C_p(mean)$ curves presented in Figure 3.14 are obtained by circumferentially averaging pressures over all the strips on the casing surface from the 3-D FLUENT simulation and those from the present panel method. Figure 3.14 shows that the pressure rise on the casing surface from the present panel method and the viscous FLUENT simulation are in good agreement.

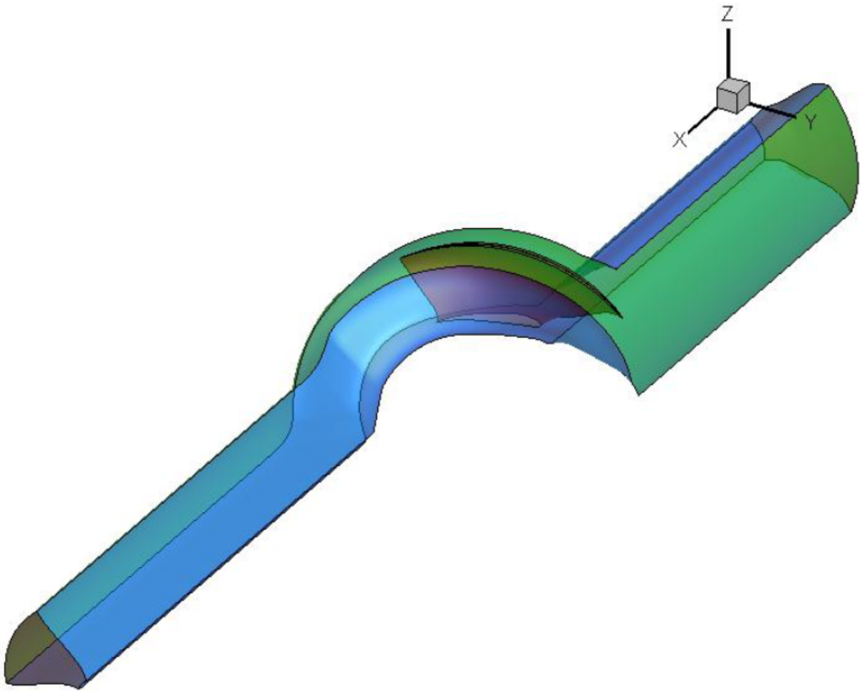

Figure 3.9: The 3D periodic mesh consisting of 2.3 million cells used for the RANS simulation. There is 0.33% gap between the casing and the rotor blade. This is the ONR-AXWJ2 rotor only system with the NACA-16 thickness blade and a sharp trailing edge.

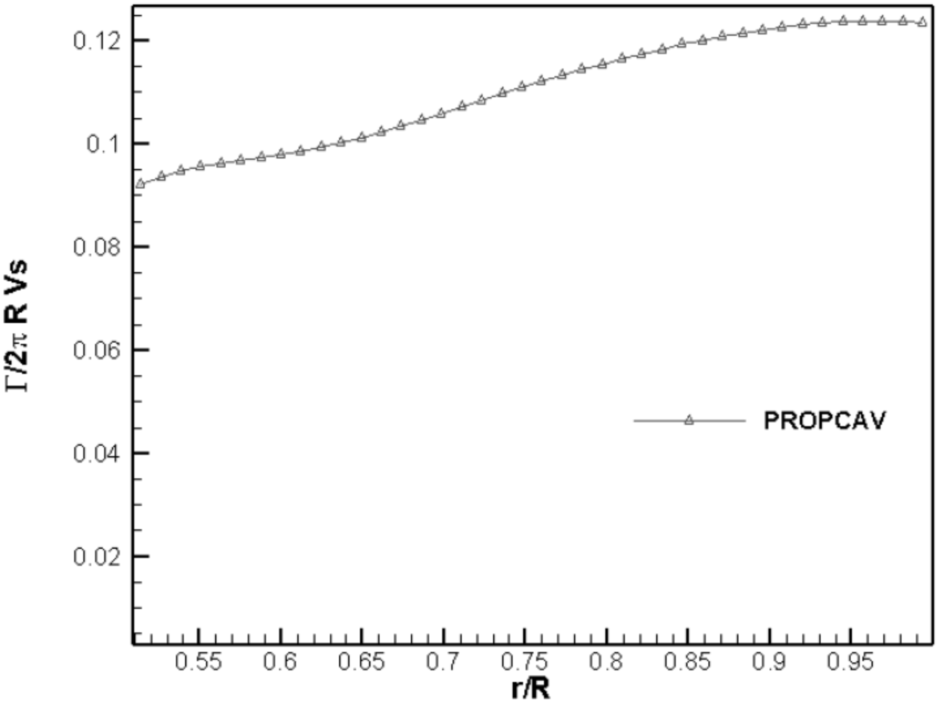

Figure 3.10: The circulation distribution on the rotor blade from the present panel method at advance coefficient $J = 1.19$.There are 120×40 panels on the blade, 90×20 panels on the hub and 160×20 panels on the casing. This is the ONR-AXWJ2 rotor only system with the NACA-16 thickness rotor blade and a sharp trailing edge.

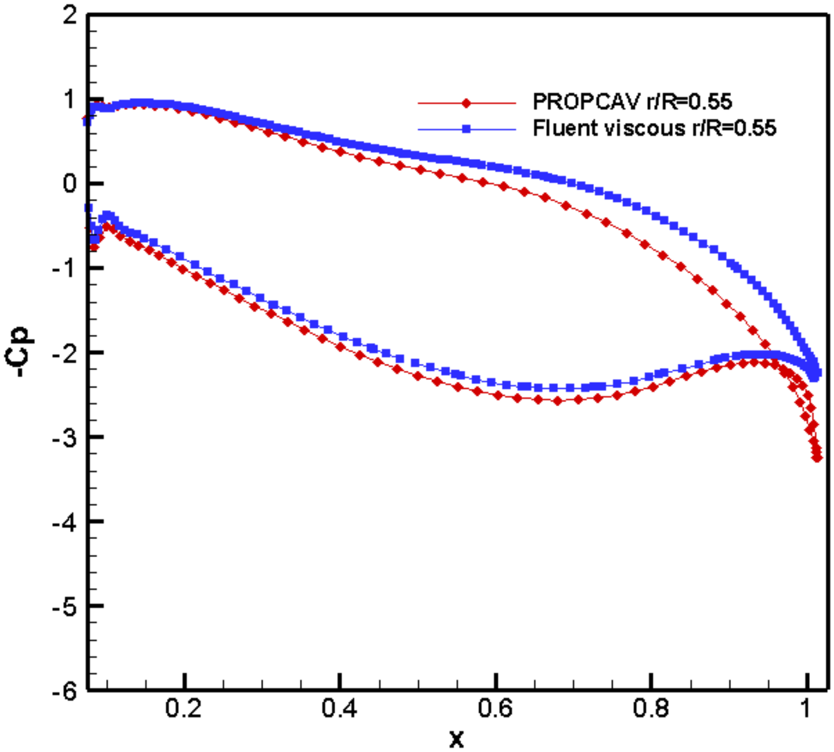

Figure 3.11: Comparison of pressure distributions on the rotor blade from the present panel method and FLUENT viscous run at advance coefficient $J = 1.19$ and radius of 0.55. There are 120×40 panels on the blade, 90×20 panels on the hub and 160×20 panels on the casing. The 3D periodic mesh has 2.3 million cells. This is the ONR-AXWJ2 rotor only system with the NACA-16 thickness rotor blade and a sharp trailing edge.

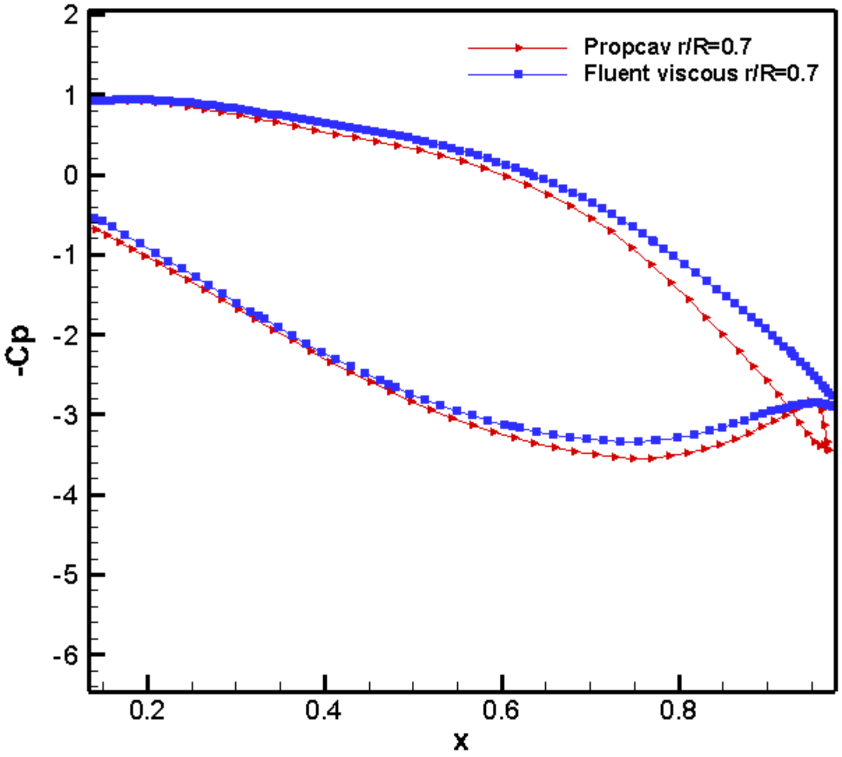

Figure 3.12: Comparison of pressure distributions on the rotor blade from the present panel method and FLUENT viscous run at advance coefficient $J = 1.19$ and radius of 0.70. There are 120×40 panels on the blade, 90×20 panels on the hub and 160×20 panels on the casing. The 3D periodic mesh has 2.3 million cells. This is the ONR-AXWJ2 rotor only system with the NACA-16 thickness rotor blade and a sharp trailing edge.

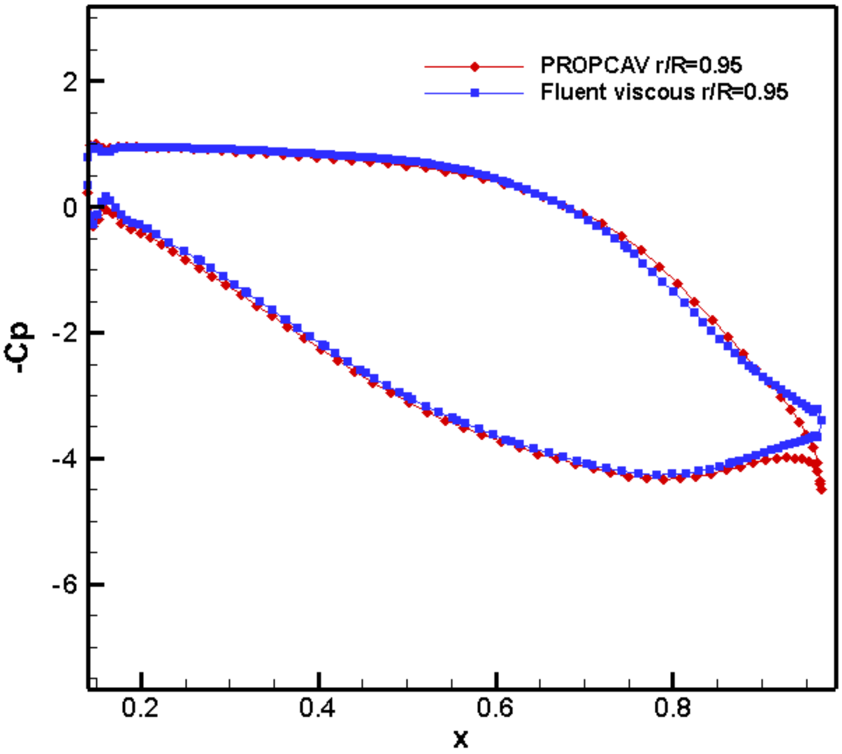

Figure 3.13: Comparison of pressure distributions on the rotor blade from the present panel method and FLUENT viscous run at advance coefficient $J = 1.19$ and radius of 0.95. There are 120×40 panels on the blade, 90×20 panels on the hub and 160×20 panels on the casing. The 3D periodic mesh has 2.3 million cells. This is the ONR-AXWJ2 rotor only system with the NACA-16 thickness rotor blade and a sharp trailing edge.

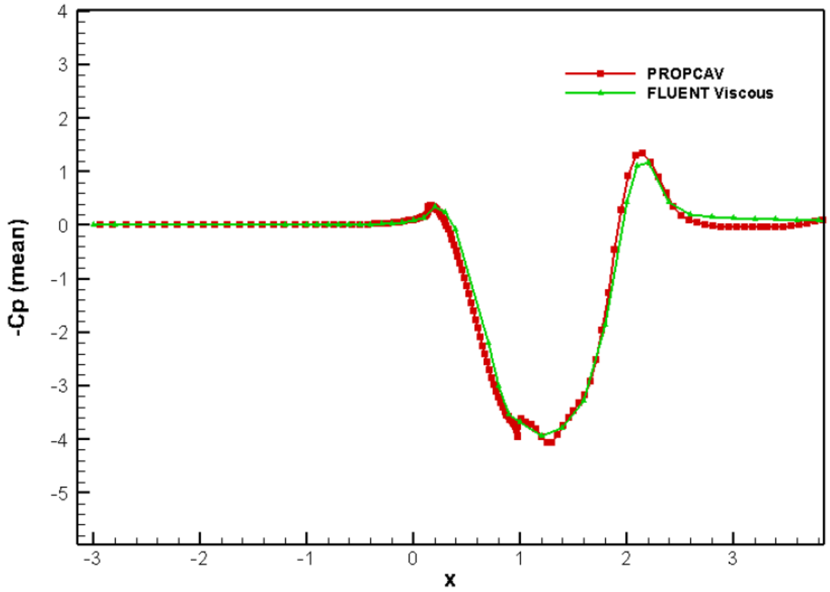

Figure 3.14: Comparison of circumferentially averaged pressure distributions on the casing surface from the present panel method and FLUENT viscous run at advance coefficient $J = 1.19$. There are 120×40 panels on the blade, 90×20 panels on the hub and 160×20 panels on the casing. The 3D periodic mesh has 2.3million cells. This is the ONR-AXWJ2 rotor only system with the NACA-16 thickness rotor blade and a sharp trailing edge.

3.3 Stator only Case

The designed stator is analyzed separately while enclosed in a cylindrical casing. The paneled geometry of the stator analysed with the present numerical method is shown in Figure 3.15.The stator is stationary and does not rotate. The present method takes 1 minute for a fully-wetted analysis by using 100 × 40 panels on the blade, 90 × 20 panels on the hub and 200 × 20 panels on the casing. The first number in the legend 100 × 40 denotes the number of panels in the chord-wise or axial direction and the second number denotes the number of elements in the span-wise direction on the blade or the circumferential direction between two blades. There is no gap between the casing and the stator blade in the simulation performed using the panel method.

The pressure distributions on the stator sections from the present panel method are compared with those from the Reynolds Averaged Navier-Stokes (RANS) solver FLUENT. A 3-D stator only periodic mesh consisting of 1.6 million cells as shown in Figure 3.16 is used to perform the RANS simulation. We have only performed inviscid simulations in FLUENT using the created mesh. The SIMPLEC scheme is used for the pressure-velocity coupling in the simulation. There is no gap between the casing and the blade in the periodic mesh. The moving wall boundary condition is used on the casing and the hub. The simulations take about 4 hours by using 16 CPUs to complete 20,000 iterations on a cluster with 2.43 GHZ quad-core 64-bit Intel Xeon processors and 16 GB of RAM.

Figures 3.17 to 3.18 show the pressure distributions on the stator blade from the present panel method and FLUENT inviscid runs at different radii. The results from the panel method are in good agreement with the RANS inviscid calculations. The circulation distribution on the stator blade from the present panel method is given in 3.19.

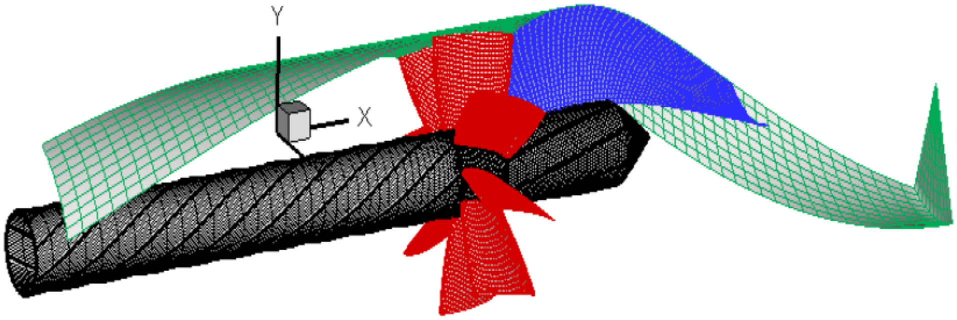

Figure 3.15: The paneled geometry of the stator only system with a 8 bladed stator. There are 100 × 40 panels on the blade, 90 × 20 panels on the hub and 200 × 20 panels on the casing. There is no gap between the casing and the blade. This is the designed stator only system with the cylindrical casing.

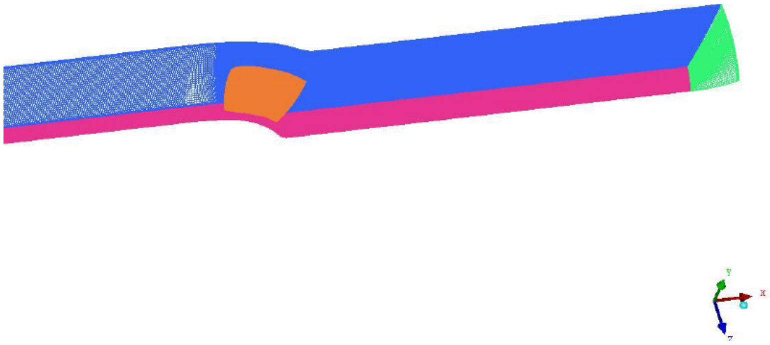

Figure 3.16: The 3D periodic mesh consisting of1.6 million cells used for the RANS simulation. There is zero gap between the casing and the stator blade. This is the designed stator only system with the cylindrical casing.

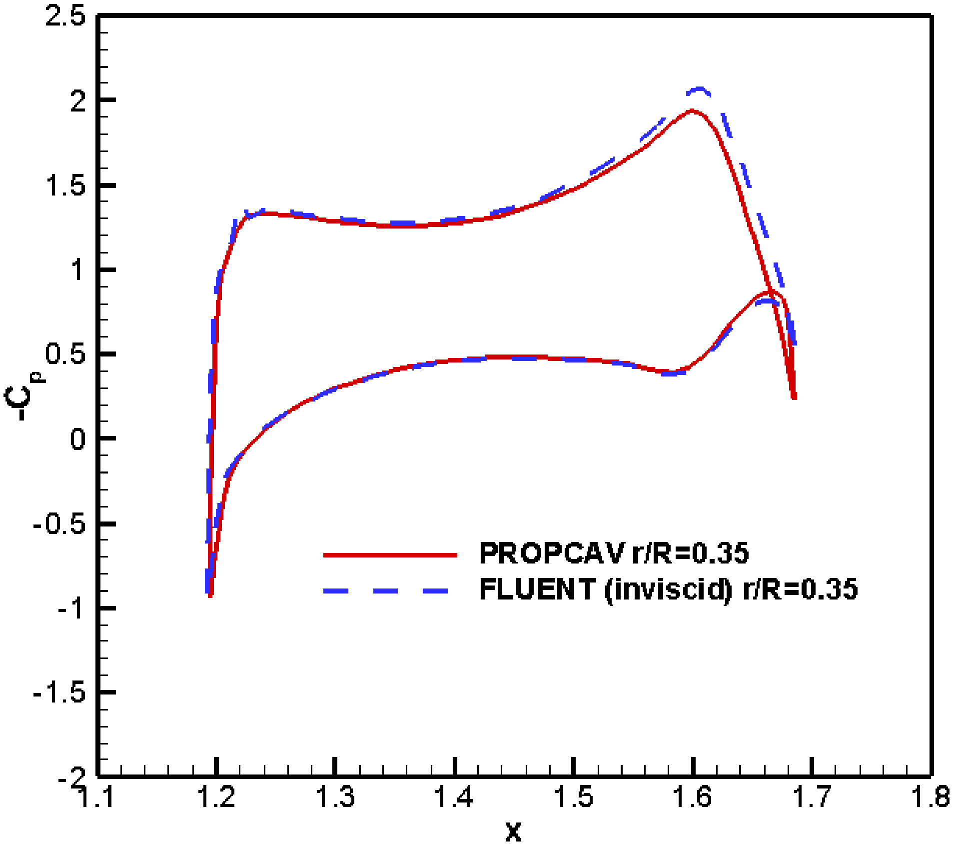

Figure 3.17: Comparison of pressure distributions on the stator blade from the present panel method and FLUENT inviscid run at advance coefficient $J = 1.00$ and radius of 0.35. There are 100×40 panels on the blade, 90×20 panels on the hub and 200×20 panels on the casing. The 3D periodic mesh has 1.6 million cells. This is the designed stator only system with the cylindrical casing.

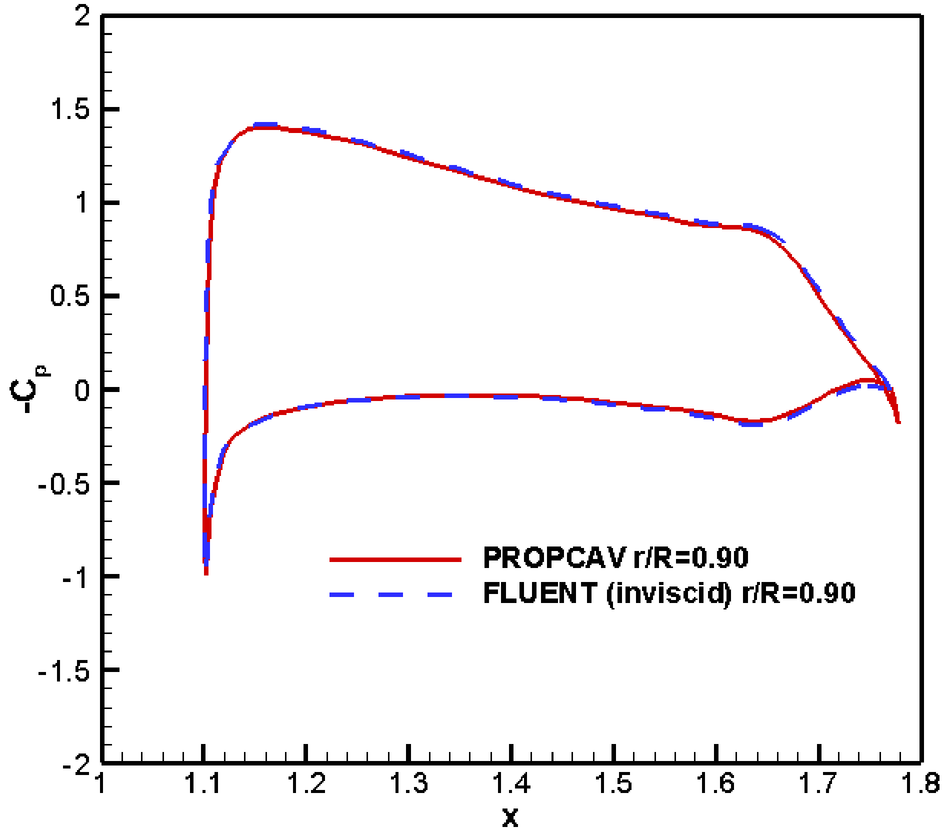

Figure 3.18: Comparison of pressure distributions on the stator blade from the present panel method and FLUENT inviscid run at advance coefficient $J = 1.00$ and radius of 0.90. There are 100×40 panels on the blade, 90×20 panels on the hub and 200×20 panels on the casing. The 3D periodic mesh has 1.6 million cells. This is the designed stator only system with the cylindrical casing.

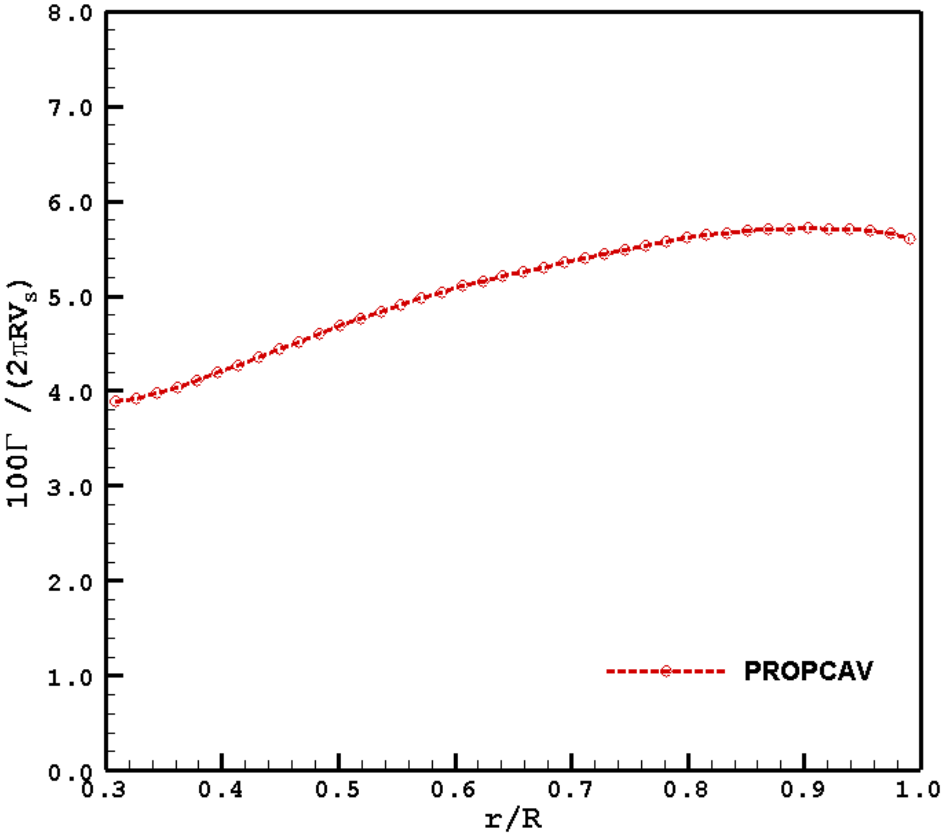

Figure 3.19: The circulation distribution on the stator blade from the present panel method at advance coefficient $J = 1.0$. There are 100×40 panels on the blade, 90×20 panels on the hub and 200×20 panels on the casing. This is the designed stator only system with the cylindrical casing.

3.4 Rotor-stator interaction

The present panel method is able to analyze the rotor only problem and the stator only problem successfully. This section presents the analysis of the interaction between the rotor and the stator in the ONR-AXWJ2 water-jet propulsion system using the induced velocity method.

The paneled geometry of the ONR-AXWJ2 water-jet system analysed with the present numerical method is shown in Figure 3.20. The present method takes about 120 minutes for 4 iterations between the rotor and stator by utilizing one CPU. There are 120 × 20 panels on the rotor and stator blades, 90 × 20 panels on the hub and 160 × 20 panels on the casing. The first number in the legend 120 × 20 denotes the number of panels in the chord-wise or axial direction and the second number denotes the number of elements in the span-wise direction on the blade or the circumferential direction between two blades. There is no gap between the casing and the blade in the simulation performed using the panel method.

A 3-D rotor-stator periodic mesh consisting of 4.2 million cells as shown in Figure 3.21 is used to perform the RANS viscous simulation. The SIMPLEC scheme is used for the pressure-velocity coupling in the simulation. There is a gap of 0.33% between the casing and the rotor blade in the periodic mesh. The realizable $k - \epsilon$ model with standard wall functions is used for the viscous simulation. The mixing plane model is utilized for the rotor-stator interaction. The stationary wall boundary condition is used on the stator blade and the moving wall boundary condition on the hub, the rotor blade and the casing. The y^+ varies from 80 to 400 on the hub and from 100 to 250 on the casing. There are 10 layers in the tip gap region of the mesh. The simulations take about 33 hours by using 32 CPUs to complete 20,000 iterations on a cluster with 2.43 GHZ quad-core 64-bit Intel Xeon processors and 16 GB of RAM. The differences between the blade geometry used in FLUENT and the present panel method are shown in 3.22.

The interactions between the rotor and the stator are performed in an iterative manner until the forces on the rotor and stator converge. Figures 3.23 to 3.24 show the convergence details of the thrust and torque coefficients on the rotor and stator respectively at advance coefficient J=1.19. The interactions between the rotor and the stator converge after two iterations. Figures 3.25 to 3.26 present the circulation distributions on the rotor and stator blades respectively at different iterations. The zeroth iteration in Figures 3.25 and 3.26 represent the rotor alone and stator alone results respectively. It is observed that the effect of the stator on the rotor loading is small whereas the effect of the rotor on the stator loading is considerable.

The $C_p(mean)$ curves presented in Figures 3.27 and 3.28 are obtained by circumferentially averaging pressures over all the strips on the casing surface from the 3-D FLUENT simulation and those from the present panel method. Figures 3.27 and 3.28 shows that the pressure rise on the casing surface from the present panel method and the viscous FLUENT simulation are in good agreement.

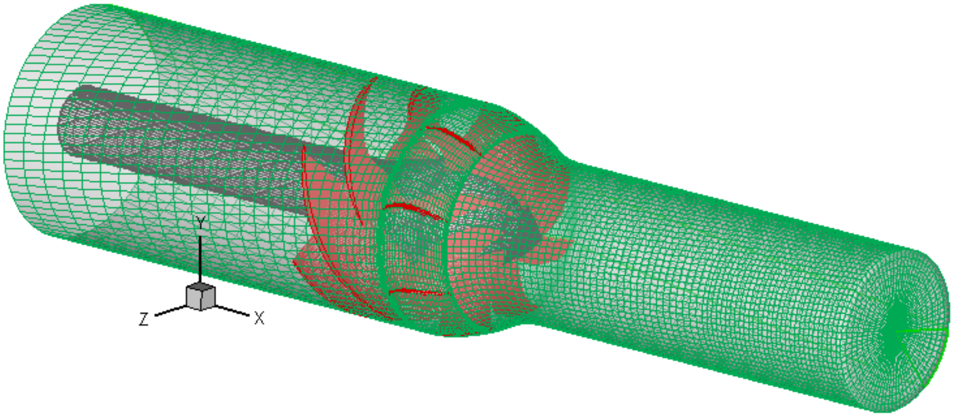

Figure 3.20: The paneled geometry of the ONR-AXWJ2 water-jet propulsion system with a 6 bladed rotor and 8 bladed stator. There are 120 × 20 panels on the rotor and stator blades, 90 × 20 panels on the hub and 160 × 20 panels on the casing. There is no gap between the casing and the blade.

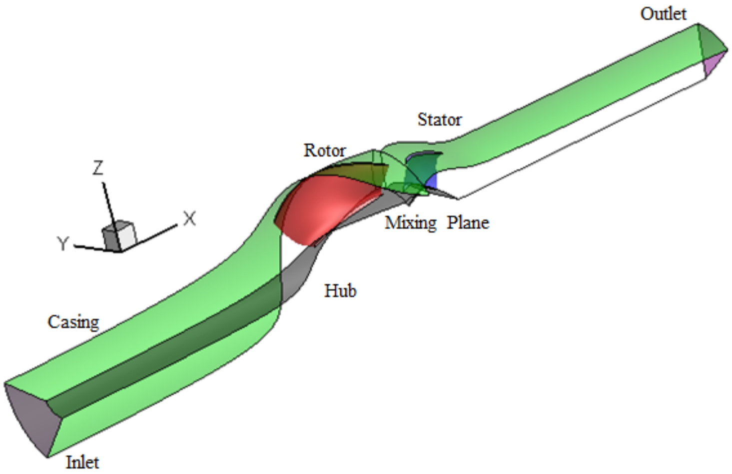

Figure 3.21: The 3D periodic mesh consisting of 4.2 million cells used for the RANS simulation of the ONR-AXWJ2 water-jet propulsion system. There is a 0.33% gap between the casing and the rotor blade.

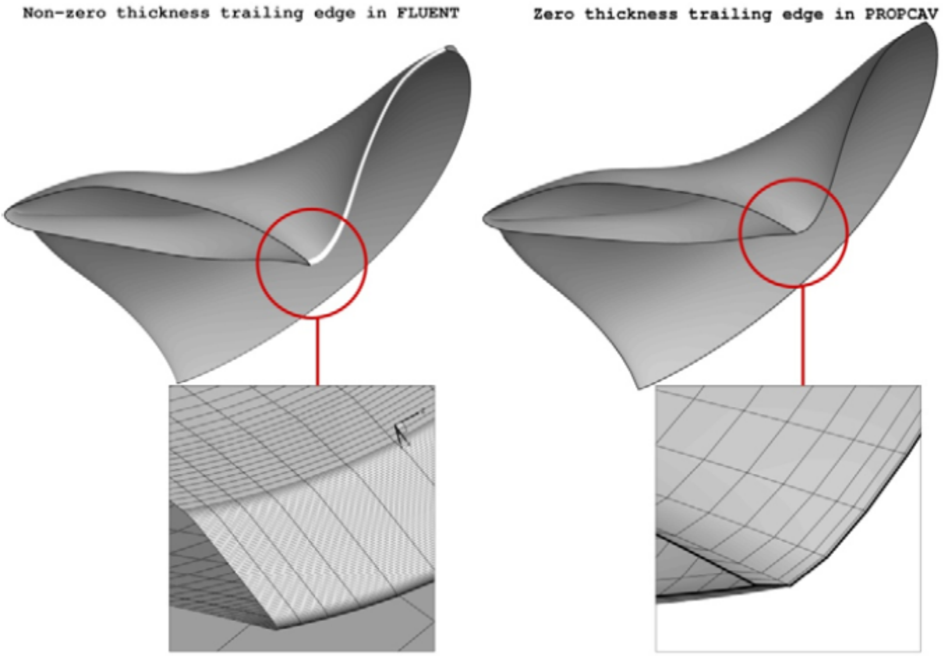

Figure 3.22: Comparison of the ONR-AXWJ2 rotor blade geometry used in the present panel method and FLUENT. The trailing edge of the rotor blade used in FLUENT is blunt and the trailing edge of the blade used in the present method is sharp with zero thickness (from Chang, 2012).

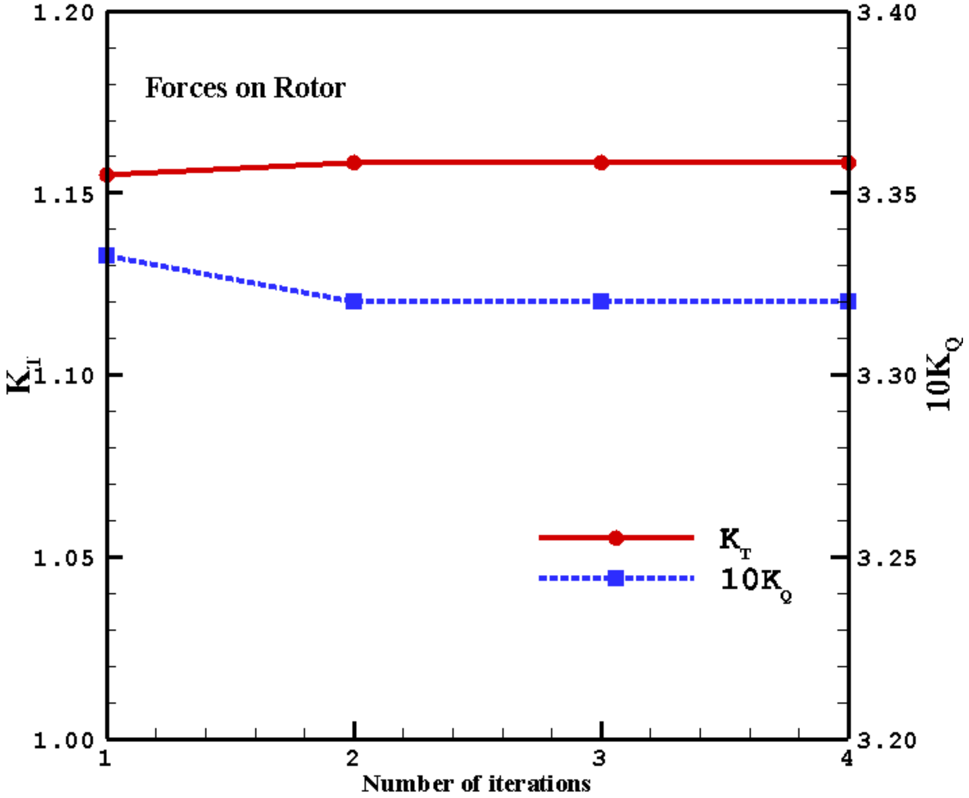

Figure 3.23: The thrust K_T and torque K_Q coefficients on the rotor blade from the present panel method at different iterations at an advance coefficient $J = 1.19$. There are 120 × 20 panels on the blade, 90 × 20 panels on the hub and 160 × 20 panels on the casing. This is the ONR-AXWJ2 water-jet propulsion system.

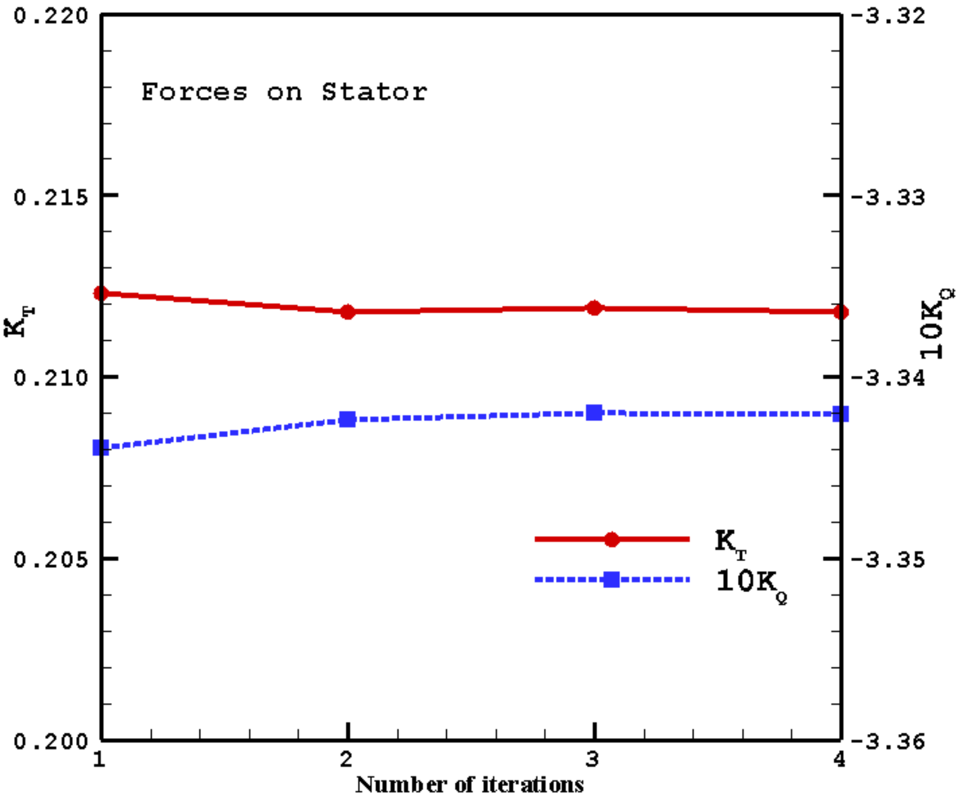

Figure 3.24: The thrust K_T and torque K_Q coefficients on the stator blade from the present panel method at different iterations at an advance coefficient $J = 1.19$. There are 120 × 20 panels on the blade, 90 × 20 panels on the hub and 160 × 20 panels on the casing. This is the ONR-AXWJ2 water-jet propulsion system.

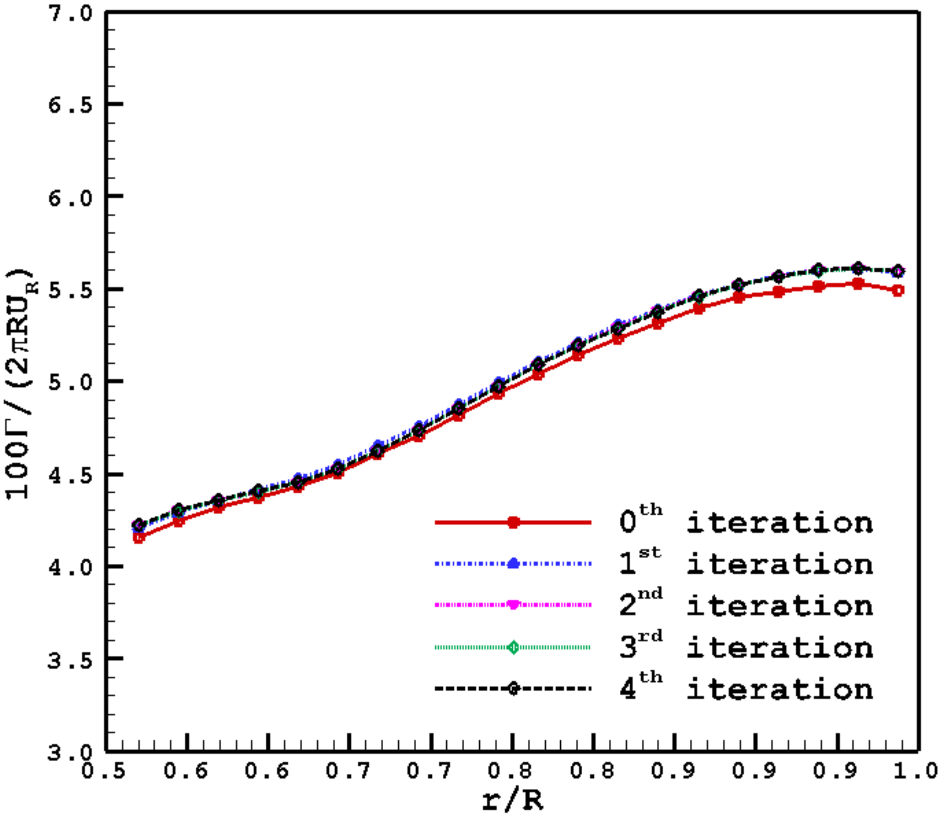

Figure 3.25: The circulation distributions on the rotor blade from the present panel method at different iterations at an advance coefficient $J = 1.19$. There are 120×20 panels on the rotor blade, 90×20 panels on the hub and 160×20 panels on the casing. This is the ONR-AXWJ2 water-jet propulsion system.

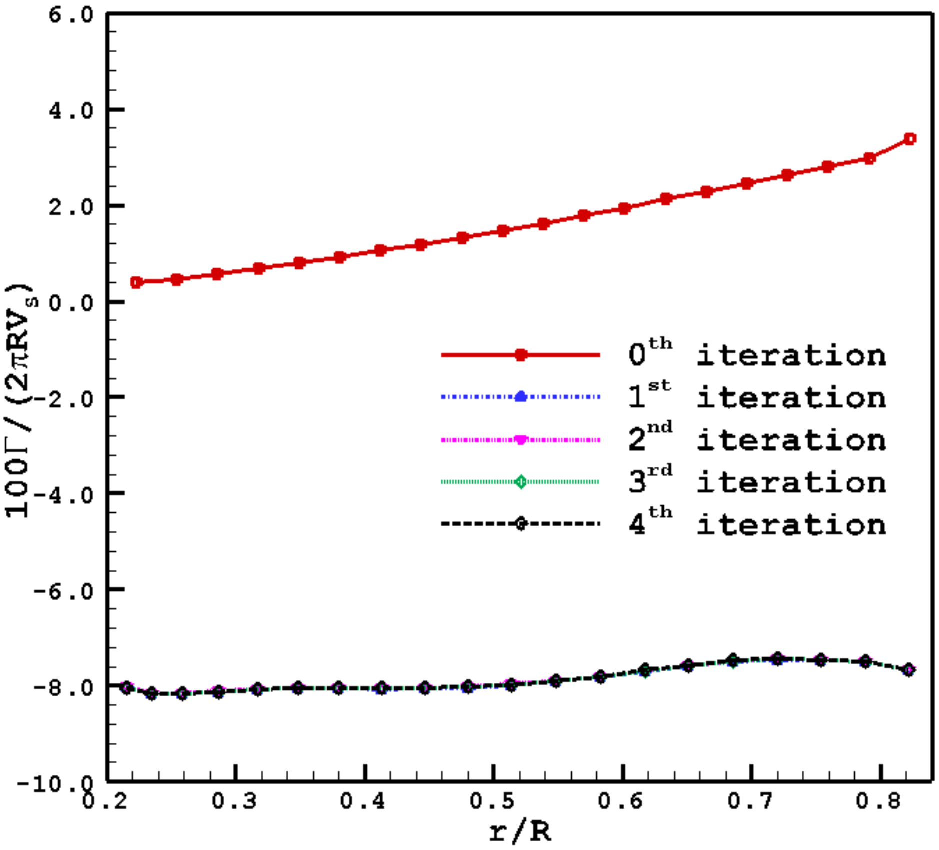

Figure 3.26: The circulation distributions on the stator blade from the present panel method at different iterations at an advance coefficient $J = 1.19$. There are 120×20 panels on the stator blade, 90×20 panels on the hub and 160×20 panels on the casing. This is the ONR-AXWJ2 water-jet propulsion system.

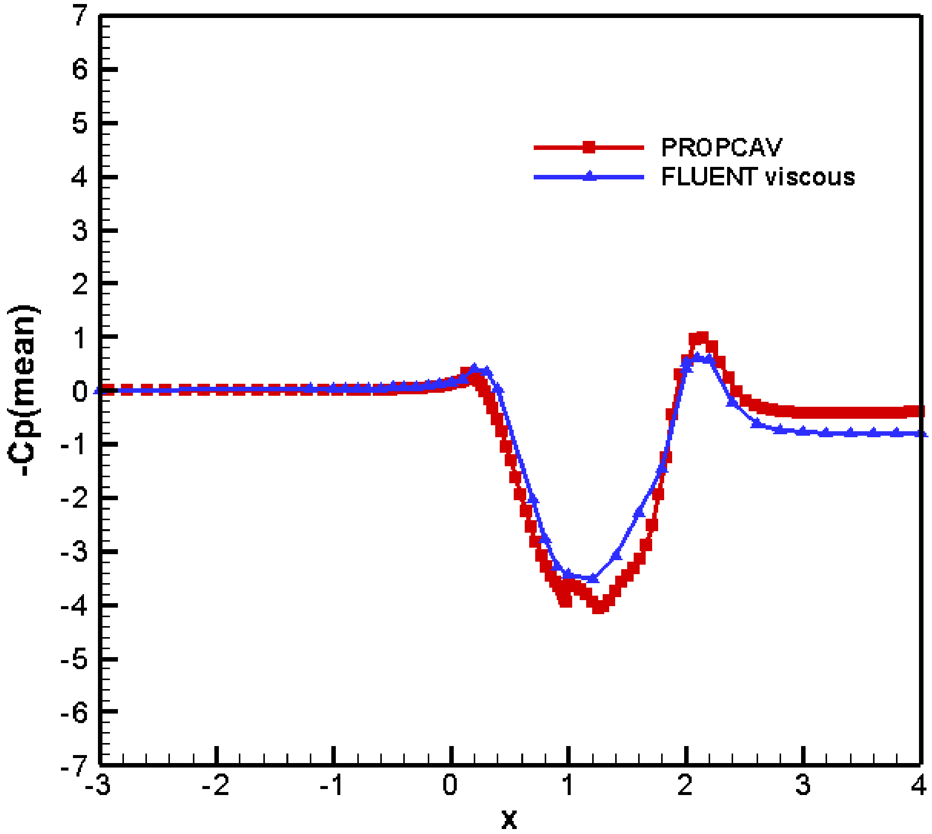

Figure 3.27: Comparison of circumferentially averaged pressure distributions on the casing surface from the present panel method and FLUENT viscous run at design advance coefficient $J = 1.19$. There are 120×20 panels on the blade, 90×20 panels on the hub and 160×20 panels on the casing. The 3D periodic mesh has 4.2 million cells. There is a 0.33% gap between the casing and the rotor blade. This is the ONR-AXWJ2 water-jet propulsion system.

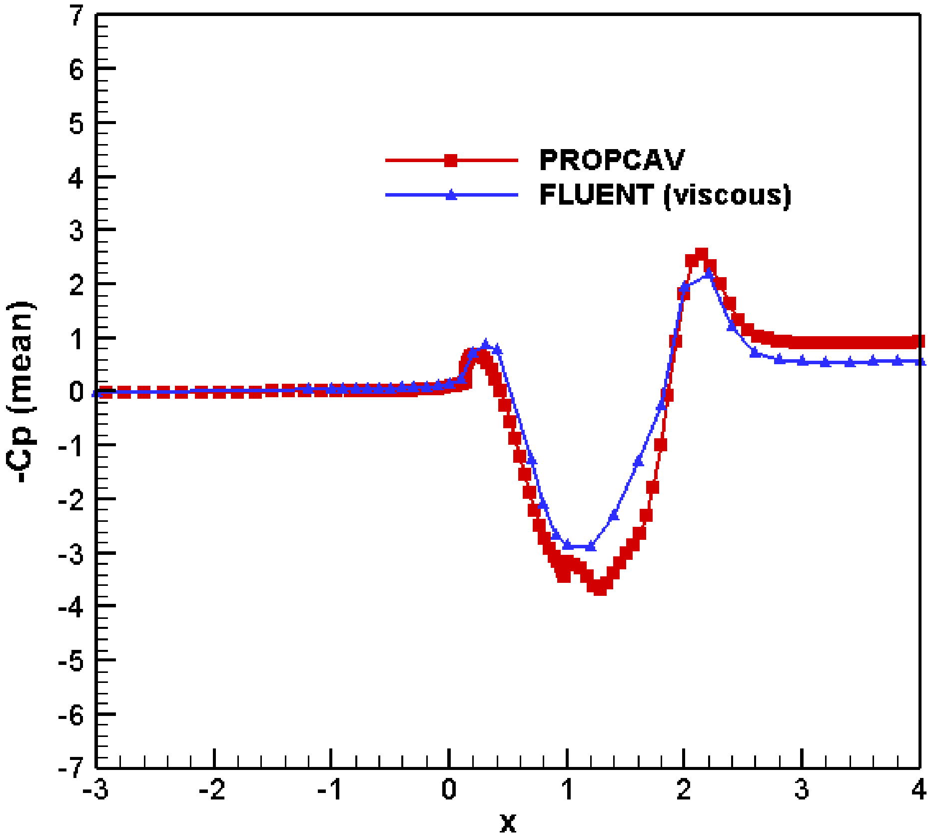

Figure 3.28: Comparison of circumferentially averaged pressure distributions on the casing surface from the present panel method and FLUENT viscous run at advance coefficient $J = 1.30$. There are 120×20 panels on the blade, 90×20 panels on the hub and 160×20 panels on the casing. The 3D periodic mesh has 4.2 million cells. There is a 0.33% gap between the casing and the rotor blade. This is the ONR-AXWJ2 water-jet propulsion system.

Chapter 4

Numerical Analysis of Inducers

The present panel method is also extended to analyze rocket engine inducers. An inducer is often used as a boost pump to raise the pressure for a subsequent impeller. The formulation and solution of the Green's integral equation for the inducer problem is the same as the rotor only problem of a water-jet system which has been presented in section 2.2.1. The present study considers inducers subject to a uniform inflow and both the wetted and the cavitating simulations are considered here.

4.1 Introduction

An inducer is an axial pump with blades that wrap in a helix around a central core as shown in Figure 4.1. Inducers are widely used in rocket engine turbo pumps to prevent cavitation in the pump main stages therefore permitting higher turbo pump operating speeds and reduced pump inlet pressure. Inducers can operate at low inlet pressures reducing the required propellant tank pressure. Low tank pressures mean lighter propellant tanks. At the same time, inducer supplies the main stage of the turbo pump with a much higher pressure than is possible by tank pressurization, thus allowing

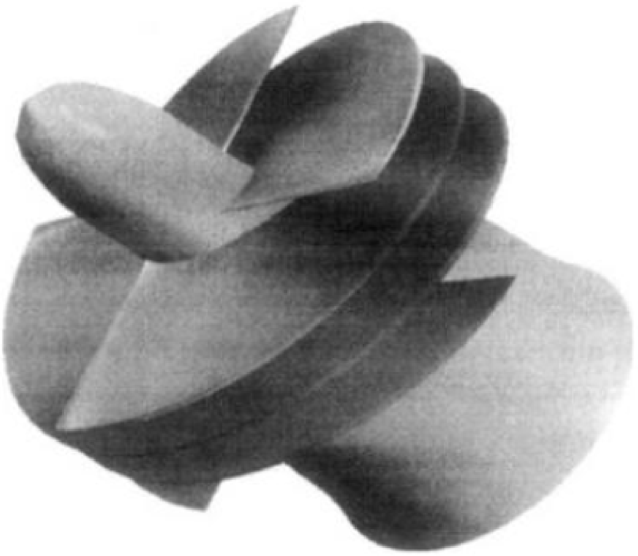

Figure 4.1: The geometrical configuration of a typical inducer used in rocket engines from Scheer et al. (1970).

the turbo pumps to operate at much higher speeds without cavitating.

4.2 Designed Inducer

This section presents the analysis of an inducer designed in-house by us, labeled the Ocean Engineering Group (OEG) inducer, to validate the numerical method. The inducer blade geometry is characterized by a low pitch to diameter ratio of 0.5. The blades wrap in a helix around a hub as shown in Figure 4.2. There are three blades in the inducer system. The design advance coefficient $J = 0.2652$ for the fully wetted condition. There is zero gap between the casing and the inducer blade in the panel method simulation.

The panel method takes 12 minutes on a single CPU for a fully-wetted analysis by using 120×20 panels on the blade, 90×20 panels on the hub and 200×20 panels on the casing. The first number in the legend 120×20 denotes the number of panels in the chord-wise or axial direction and the second number denotes the number of elements in the span-wise direction on the blade or the circumferential direction between two blades.

The pressure distributions on the inducer blade sections from the present panel method are compared with those from the RANS solver FLUENT. A 3-D periodic mesh consisting of 3.6 million cells as shown in Figure 4.3 is used to perform the RANS simulation. The SIMPLEC scheme is used for the pressure-velocity coupling in the simulation. The $k - \omega$ SST model is used for the viscous simulation. The moving wall boundary condition is used on the casing and the hub. The y^+ varies from 40 to 380 on the hub and from 50 to 200 on the casing. The simulations take about 12 hours by using 16 CPUs to complete 20,000 iterations on a cluster with 2.43 GHZ quad-core 64-bit Intel Xeon processors and 16 GB of RAM.

Figures 4.5 to 4.7 show the pressure distributions on the inducer blade from the present panel method and FLUENT viscous runs at different radii. The results from the panel method are in very good agreement with the RANS viscous calculations. The circulation distribution on the inducer blade from the present panel method is given in 4.4.

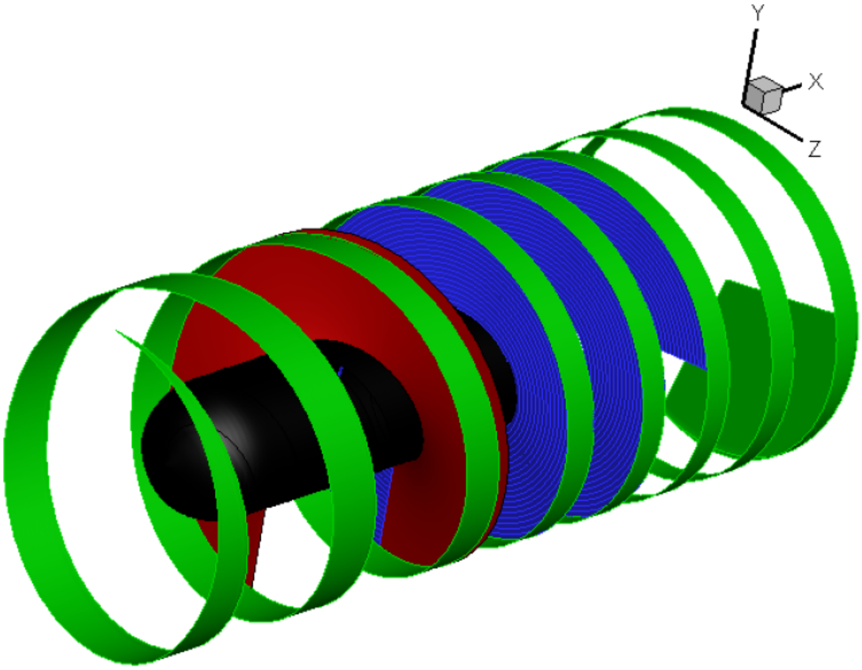

Figure 4.2: The paneled geometry of the OEG inducer system with a 3 bladed inducer. There are 120 × 20 panels on the blade, 90 × 20 panels on the hub and 200 × 20 panels on the casing. There is zero gap between the casing and the inducer blade in the simulation.

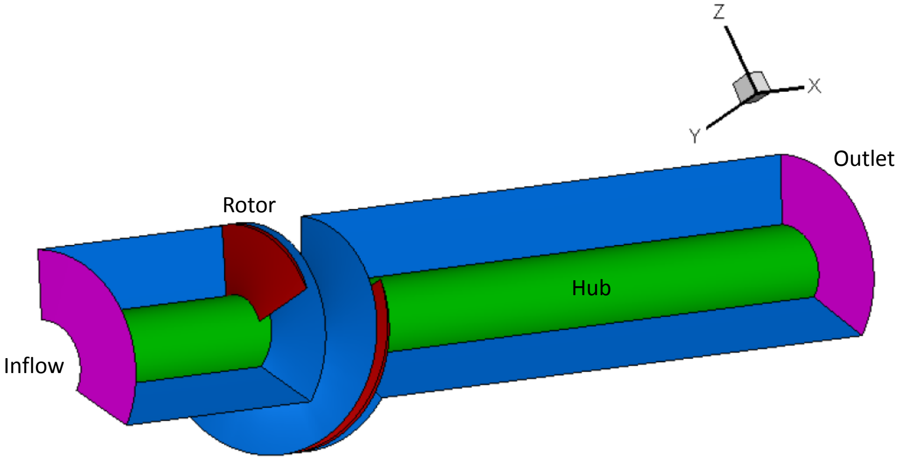

Figure 4.3: The 3D periodic mesh consisting of 3.6 million cells used for the RANS simulation. There is zero gap between the casing and the OEG inducer blade in the simulation.

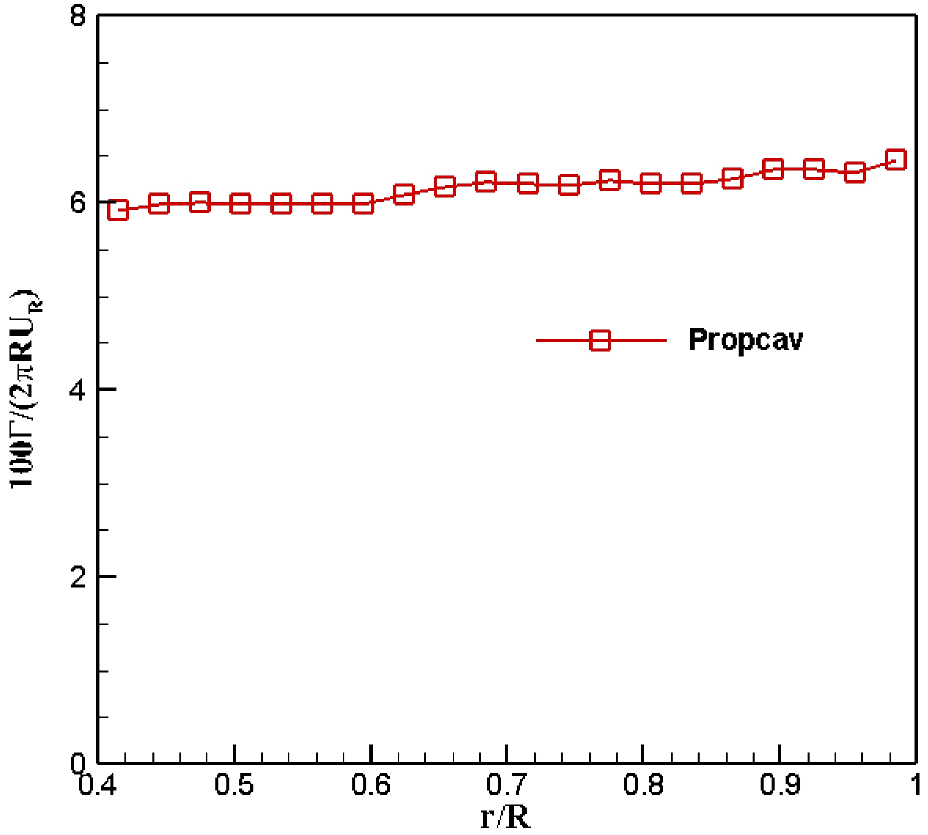

Figure 4.4: The circulation distribution on the OEG inducer blade from the present panel method at advance coeffficient $J = 0.2652$. There are 120×20 panels on the blade, 90×20 panels on the hub and 200×20 panels on the casing.

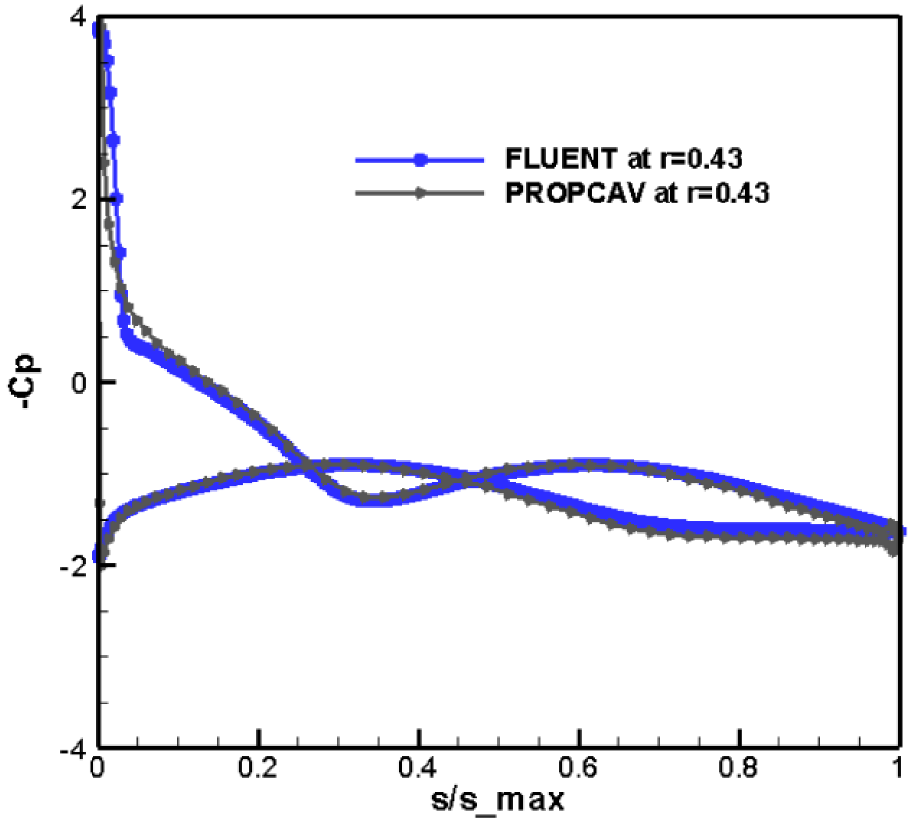

Figure 4.5: Comparison of pressure distributions on the OEG inducer blade from the present panel method and FLUENT viscous run at advance coefficient $J = 0.2652$ and radius of 0.43. There are 120×20 panels on the blade, 90×20 panels on the hub and 160×20 panels on the casing. The 3D periodic mesh has 2.3 million cells.

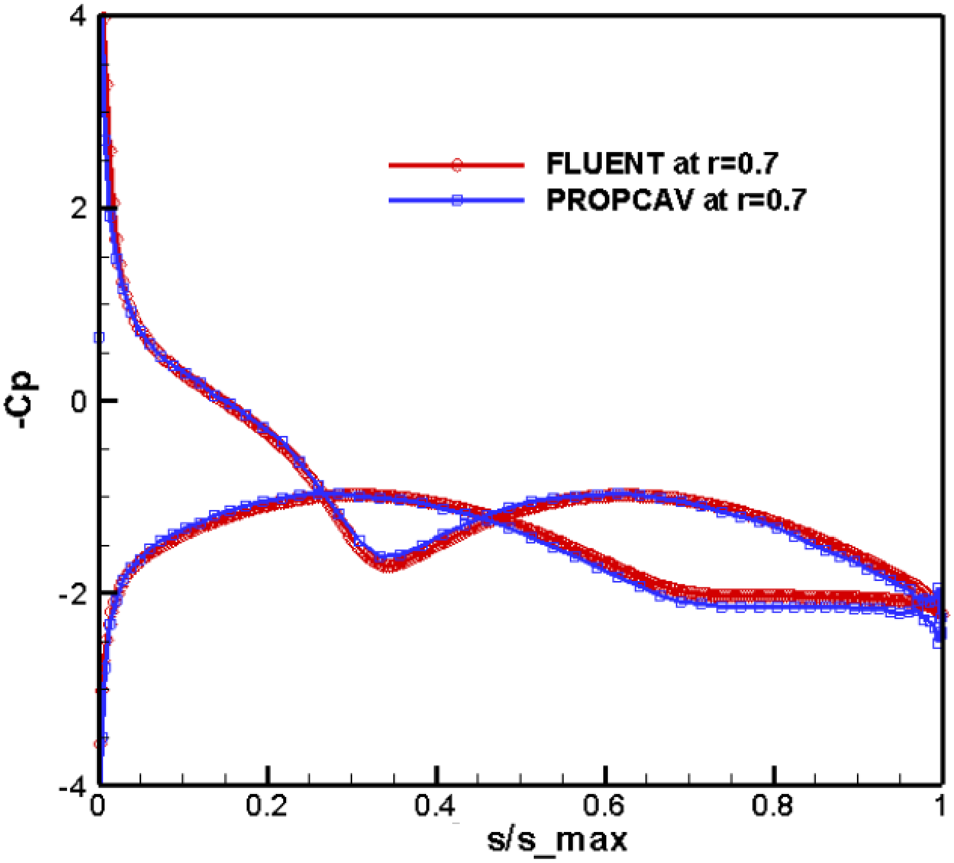

Figure 4.6: Comparison of pressure distributions on the OEG inducer blade from the present panel method and FLUENT viscous run at advance coefficient $J = 0.2652$ and radius of 0.70. There are 120×20 panels on the blade, 90×20 panels on the hub and 200×20 panels on the casing. The 3D periodic mesh has 2.3 million cells.

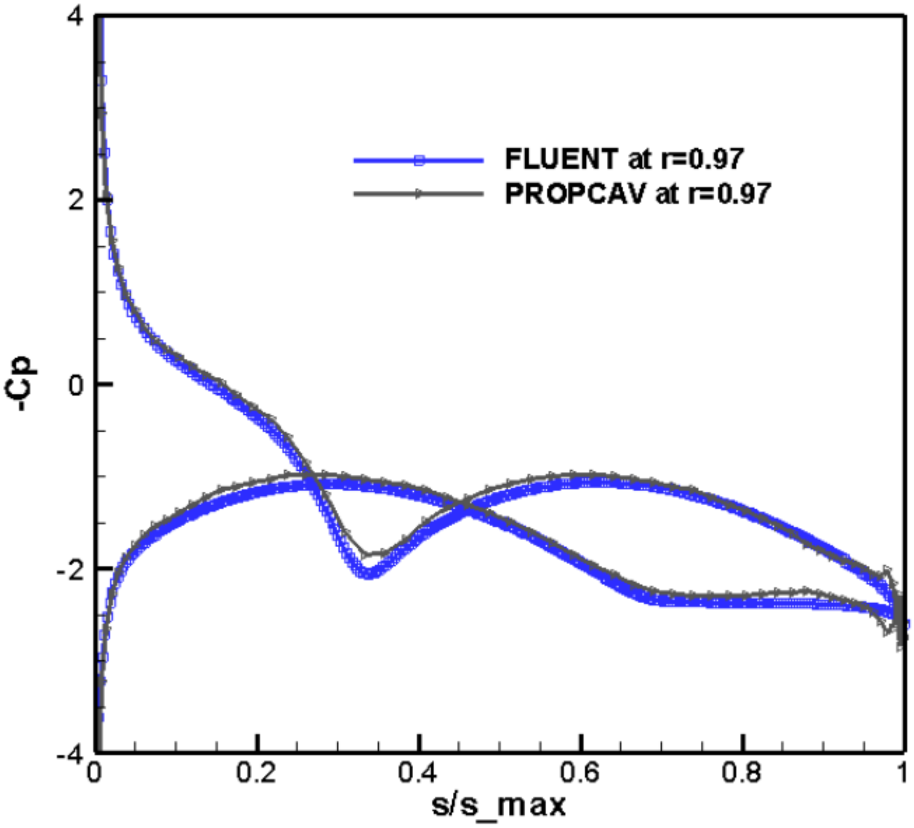

Figure 4.7: Comparison of pressure distributions on the OEG inducer blade from the present panel method and FLUENT viscous run at advance coefficient $J = 0.2652$ and radius of 0.97. There are 120×20 panels on the blade, 90×20 panels on the hub and 200×20 panels on the casing. The 3D periodic mesh has 2.3 million cells.

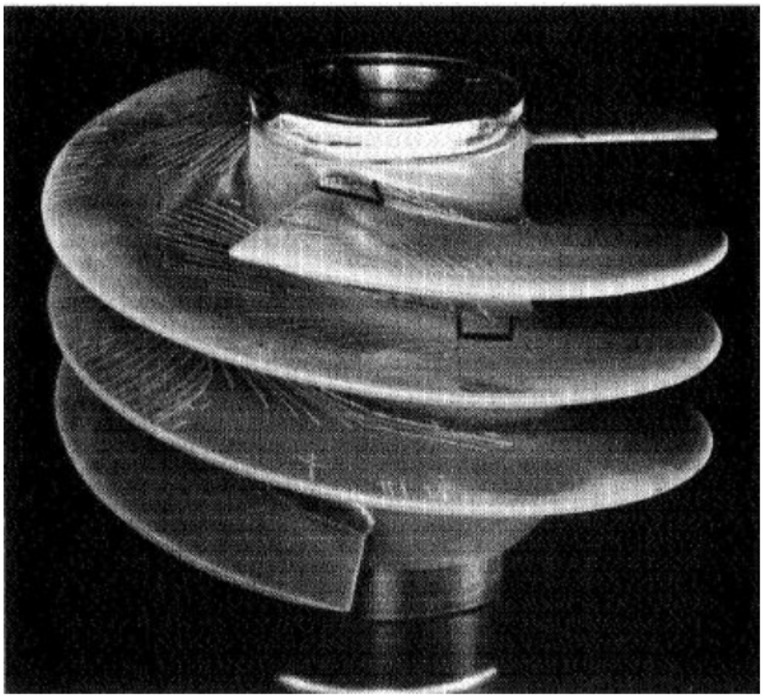

Figure 4.8: The fabricated inducer from Scheer et al. (1970). The operating conditions are at flow coefficient of 0.0084 which corresponds to an advance coefficient $J = 0.2652$, 100% speed and a net positive suction head (NPSH) of 32.3 m.

4.3 Industry Inducer

This inducer representative of typical rocket engine inducers was designed, fabricated and tested to provide measurements of blade surface pressures and stresses by Scheer et al. (1970) as shown in Figure 4.8. The operating conditions are at flow coefficient of 0.0084 which corresponds to an advance coefficient $J = 0.2652$, 100% speed and a net positive suction head (NPSH) of 32.3 m.

The paneled geometry of the industry inducer system analyzed with the present panel method is shown in Figure 4.9. The present method takes 12 minutes on a single CPU for a fully-wetted analysis by using 120 × 20 panels on the blade, 90 × 20 panels on the hub and 200 × 20 panels on the casing. There is no gap between the casing and the blade in the simulation performed using the panel method. The real size of the gap is 0.60% of the blade radius but the gap is chosen to be sealed in the present approach since the tip gap effect is not significant to the overall performance. The steady fully wetted performance of the inducer subject to a uniform inflow is studied here.

The industry blade geometry provided to us is essentially constant thickness, which suddenly tapers off at the leading and trailing edges as shown in Figure 4.10. This introduces camber which can affect the pressure distributions. Hence to ensure that there is no camber, we have modified the industry blade sections. The new blade is created using the smooth lower curve shown in Figure 4.10 as the centerline. The new blade section given in Figure 4.11, has no camber and constant thickness everywhere except at the leading and trailing edges where they are closed with elliptic ends.

The pressure distributions obtained from the present panel method are compared with the experimental and RANS results at the tip radius $r/R = 0.94$ and mean radius $r/R = 0.68$.The experimental results are obtained from the report prepared by Scheer et al. (1970). The pressure is expressed in terms of the static head coefficient defined as

$$\psi_s = \frac{g(p - p_{T_o})}{\rho U_T^2} \tag{4.1}$$

where p is the local static pressure, p_{T_o} is the inlet total pressure and U_T is the rotor tip speed.

The predicted circulation from the present panel method is positive and nearly constant as shown in Figure 4.12. Figures 4.13 and 4.14 show the pressure distributions on the inducer blade from the present panel method and experiments at the mean radius and the tip radius respectively. The results from the panel method are in reasonable agreement with the experimental results.

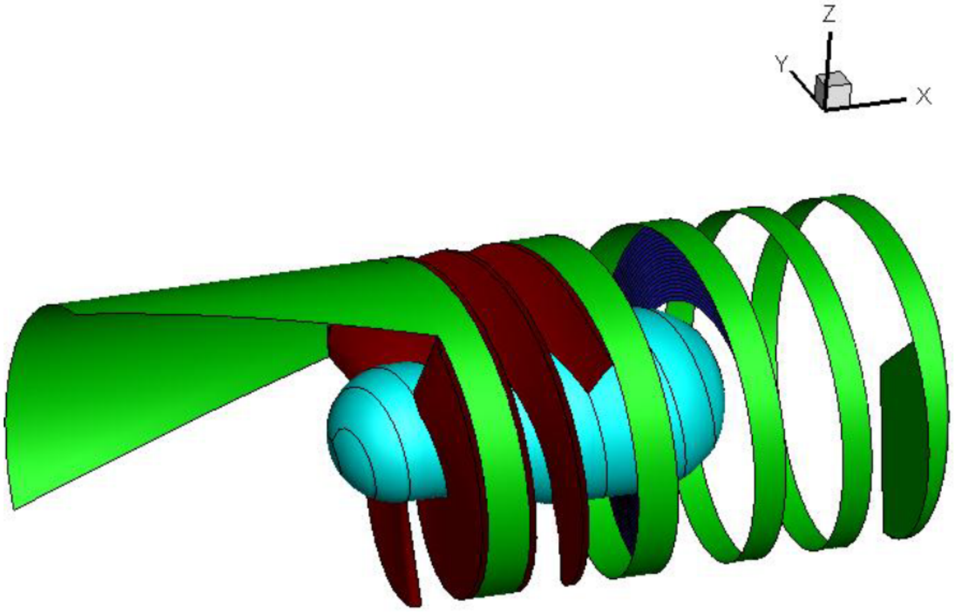

Figure 4.9: The paneled geometry of the industry inducer system with a 3 bladed blade. There are 120 × 20 panels on the blade, 90 × 20 panels on the hub and 200 × 20 panels on the casing. There is zero gap between the casing and the inducer blade.

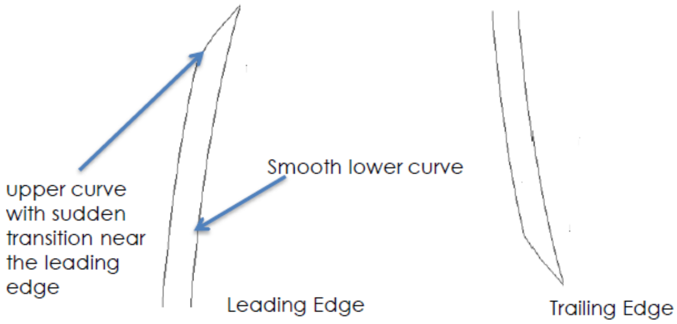

Figure 4.10: The original industry inducer blade geometry is essentially constant thickness which suddenly tapers off at the leading and trailing edges.

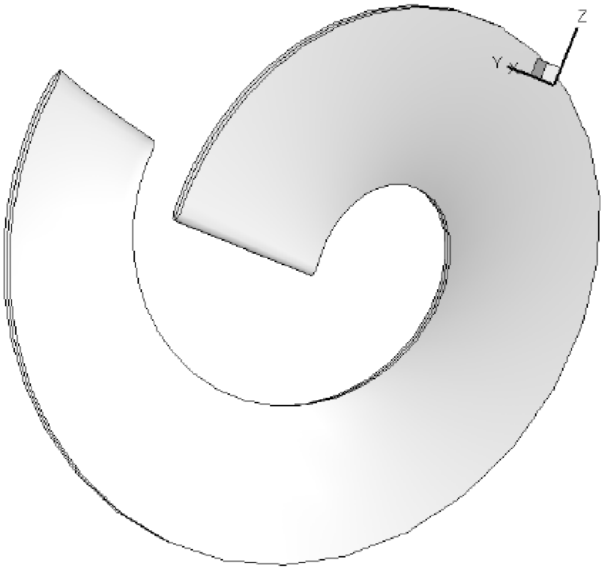

Figure 4.11: The new blade section of the industry inducer with no camber and constant thickness everywhere except at the leading and trailing edge where they are closed with elliptic ends. Hence it is a constant thickness blade for 97 % of the chord length.

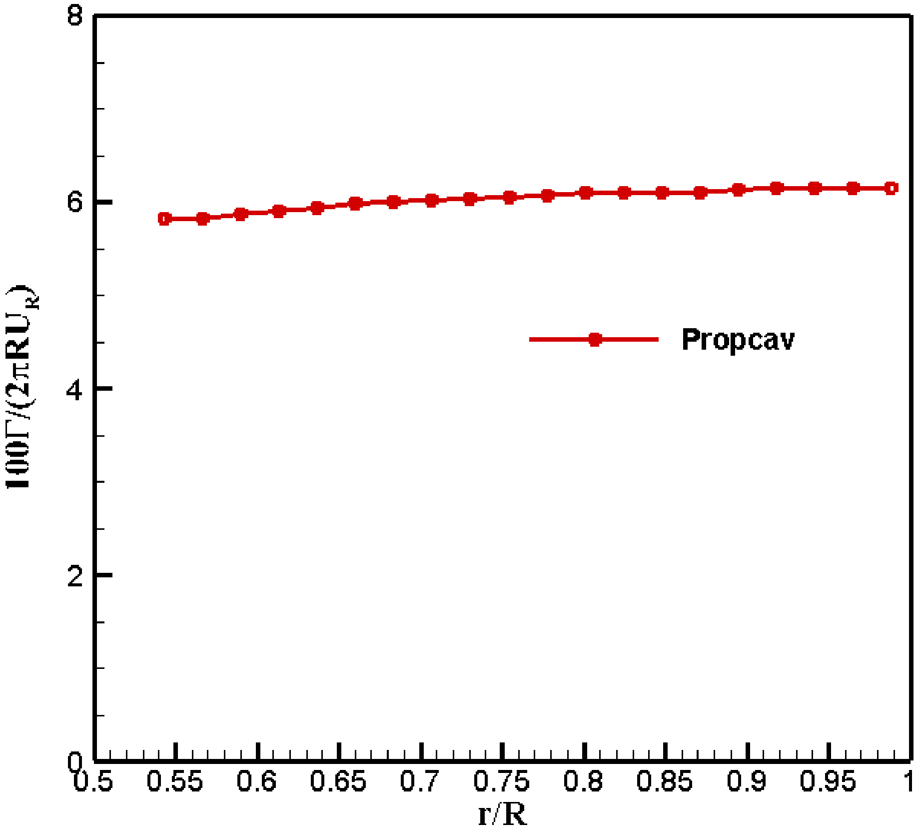

Figure 4.12: The circulation distribution on the industry inducer blade from the present panel method at advance coefficient $J = 0.2652$.There are 120×20 panels on the blade, 90×20 panels on the hub and 200×20 panels on the casing.

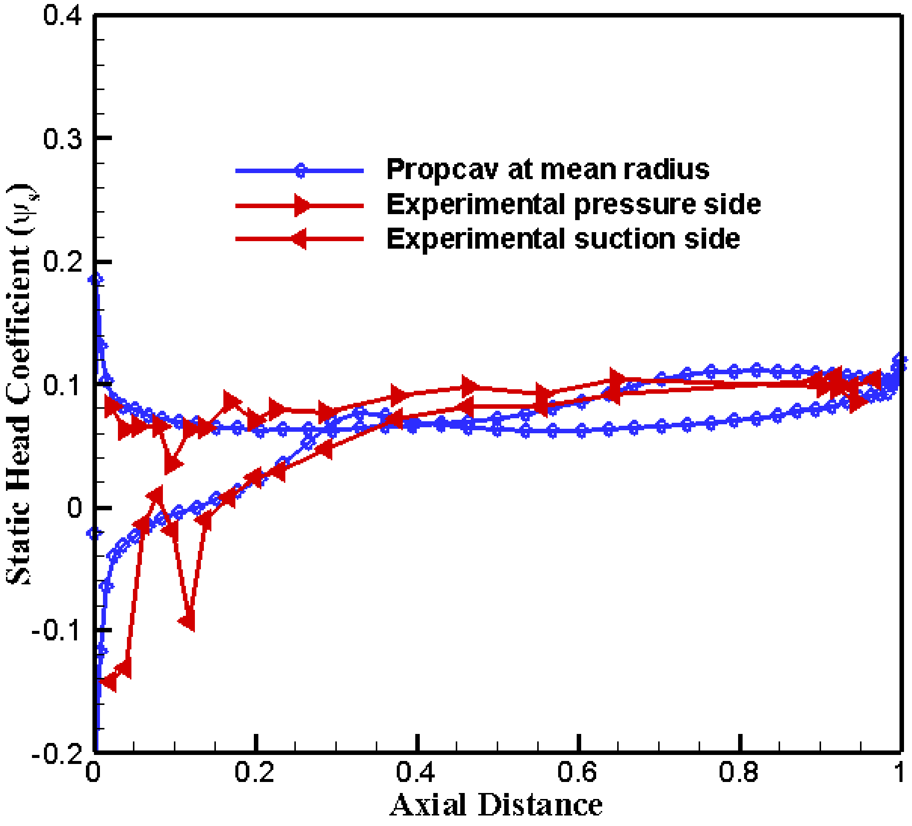

Figure 4.13: Comparison of pressure distributions on the industry inducer blade from the present panel method and experimental results at advance coeffficient $J = 0.2652$ and mean radius of 0.68. There are 120×20 panels on the blade, 90×20 panels on the hub and 200×20 panels on the casing.The experimental results are obtained from Scheer et al. (1970).

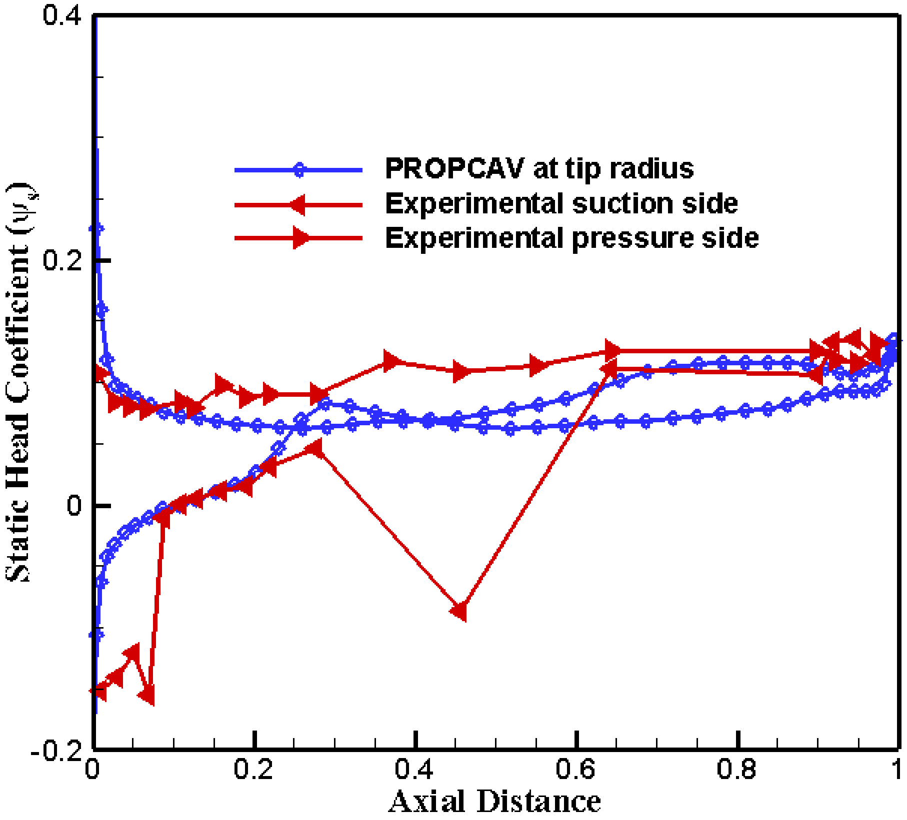

Figure 4.14: Comparison of pressure distributions on the industry inducer blade from the present panel method and experimental results at advance coefficient $J = 0.2652$ and tip radius of 0.94. There are 120 × 20 panels on the blade, 90 × 20 panels on the hub and 200 × 20 panels on the casing.The experimental results are obtained from Scheer et al. (1970).

4.4 Cavitating runs

Cavitating simulations are also performed for the industry inducer at a cavitation number $\sigma = 2.8977$ and advance coefficient $J = 0.2652$. The cavitation number is defined as

$$\sigma = \frac{p - p_v}{0.5 \rho U^2} \tag{4.2}$$

where p is the local static pressure, p_v is the vapor pressure and U is the inflow speed.

The present method takes 16 minutes on a single CPU for a cavitating analysis by using 120×20 panels on the blade, 90×20 panels on the hub and 200×20 panels on the casing. The circulation from the cavitating and fully wetted simulations are shown in Figure 4.15. Figures 4.16 and 4.17 show the pressure distributions on the inducer blade from the cavitating and fully wetted analysis at the mean radius and the tip radius respectively. The cavity shapes on the inducer blade from the cavitating simulation are given in Figure 4.18. The cavities are only present near the leading edge on the suction side of the inducer blade in the cavitating simulation.

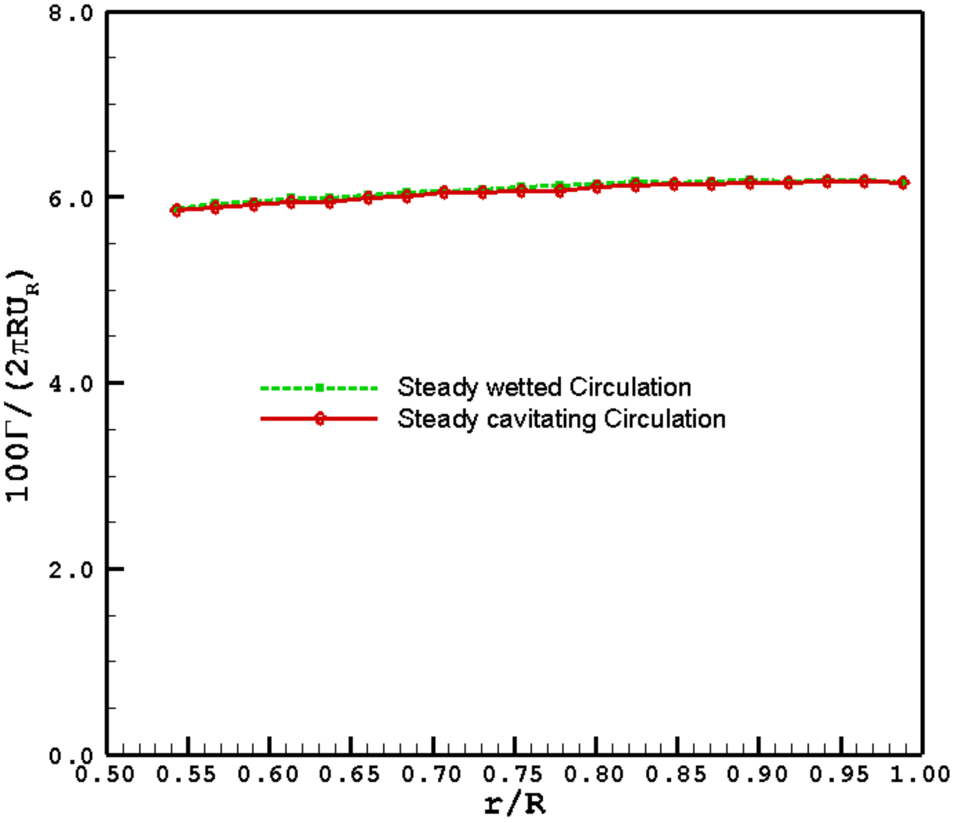

Figure 4.15: The predicted circulation distribution on the industry inducer blade from the cavitating and fully wetted simulations using the present panel method at an advance coeffficient $J = 0.2652$ and $\sigma = 2.8977$ .There are 120×20 panels on the blade, 90×20 panels on the hub and 200×20 panels on the casing.

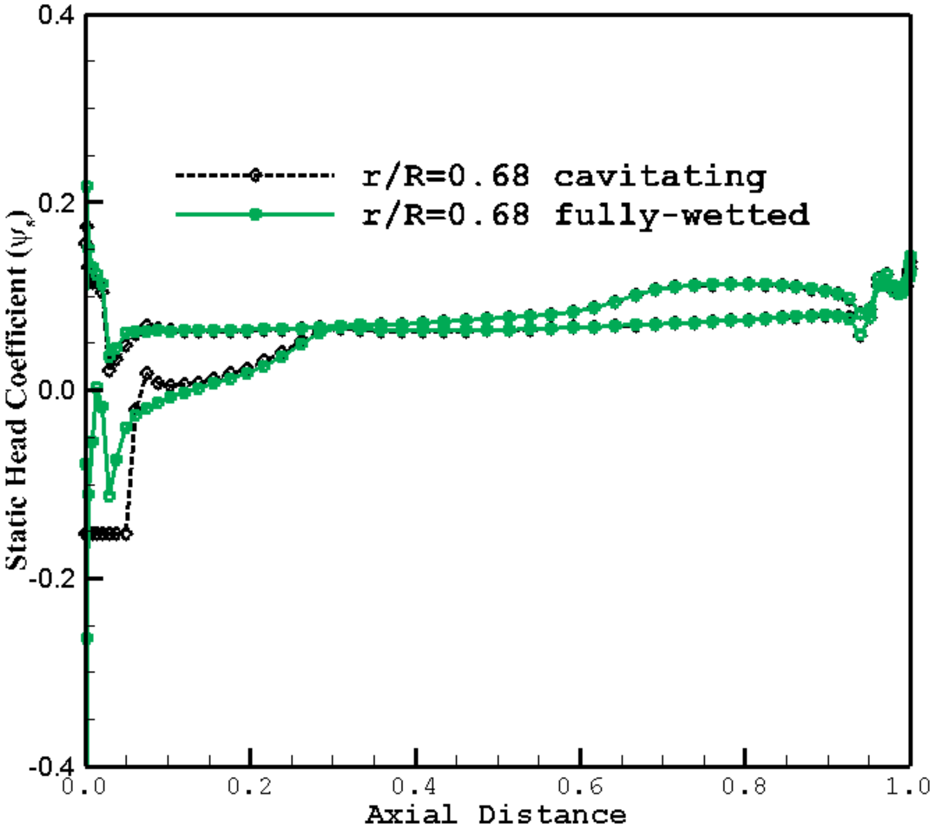

Figure 4.16: Comparison of pressure distributions on the industry inducer blade from the cavitating and fully wetted analysis using the present panel method at an advance coefficient $J = 0.2652$, $\sigma = 2.8977$ and mean radius of 0.68. There are 120 × 20 panels on the blade, 90 × 20 panels on the hub and 200 × 20 panels on the casing.

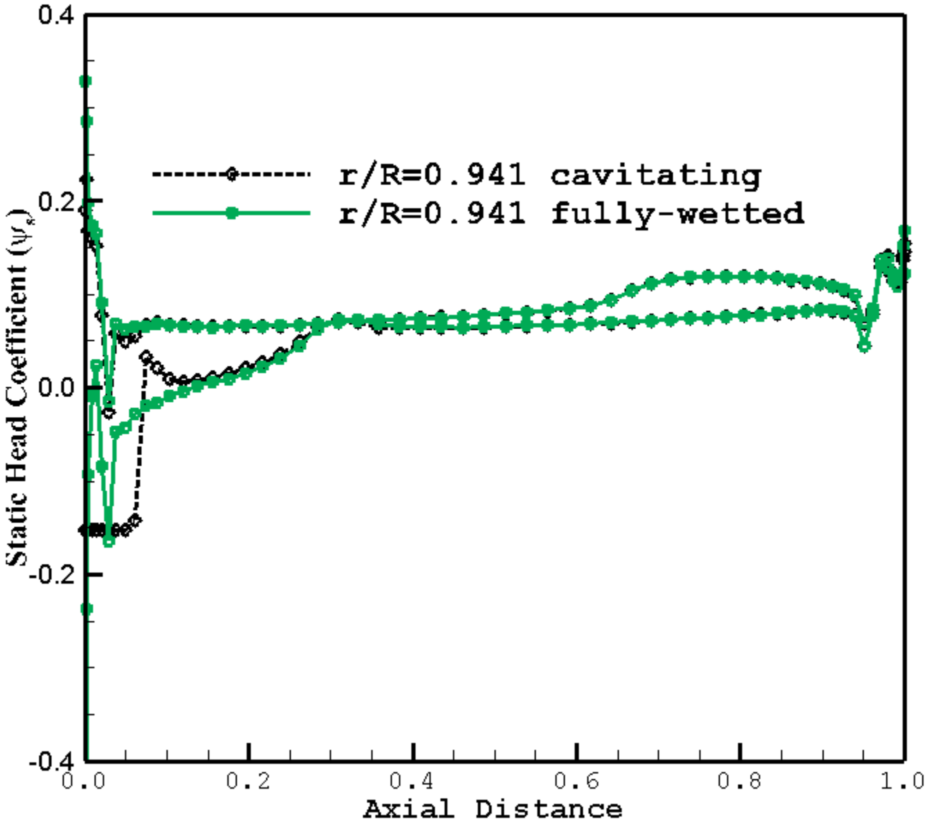

Figure 4.17: Comparison of pressure distributions on the industry inducer blade from the cavitating and fully wetted analysis using the present panel method at an advance coefficient $J = 0.2652$, $\sigma = 2.8977$ and tip radius of 0.94. There are 120×20 panels on the blade, 90×20 panels on the hub and 200×20 panels on the casing.

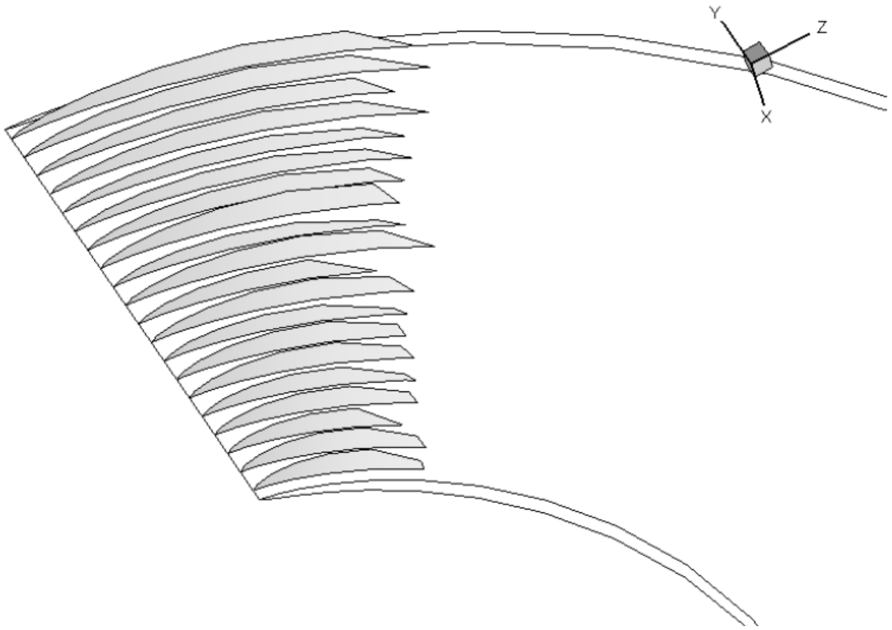

Figure 4.18: The cavities at the leading edge on the suction side of the industry inducer blade from the present panel method at $J = 0.2652$ and $\sigma = 2.8977$. There are 120×20 panels on the blade, 90×20 panels on the hub and 200×20 panels on the casing.

Chapter 5

Conclusions and future work

This chapter presents the conclusions derived from my research and outlines the direction of the future work.

5.1 Conclusions

A numerical panel method based on inviscid irrotational flow theory and utilizing hyperboloid panels has been developed and successfully applied for the simulation of steady fully wetted flows inside water-jet pumps and rocket engine inducers.

The source and dipole influence coefficients of non-planar hyperboloid panels are accurately computed using Gauss quadrature. The numerical scheme is validated by evaluating the influence coefficients for a non-planar quadrilateral as well as the simplified case of a water-jet casing problem.

The numerical panel method is improved significantly to predict the hydrodynamic performance parameters of a water-jet propulsion system. The present method solves the boundary value problem subject to a uniform inflow directly by simulating the blade, casing/shroud and hub geometries as discretized panels. The Green's integral equation and the influence coefficients for the water-jet/inducer problem are defined and solved by spreading constant strength dipoles and sources on the blade, hub and casing surfaces and constant strength dipoles on the shed wake sheets behind the rotor/ stator blades. The circulation and pressure distributions for the rotor alone problem and the stator alone problems are found to be in good agreement with RANS calculations obtained using FLUENT. The pressure rise on the casing is successfully estimated for the rotor only case using the numerical panel method.

The rotor- stator interaction is accomplished using an iterative procedure which considers the effect of circumferentially averaged induced velocities between the rotor and the stator. The iterations for the rotor-stator problem converge quickly. The influence of the stator on the rotor loading is observed to be small. The pressure rise on the casing for the ONR-AXWJ2 water-jet propulsion system is obtained using the numerical panel method and is in good agreement with the FLUENT results. The panel method also requires significantly less computational time compared to RANS solvers.

The numerical panel method is also successfully extended to analyze rocket engine inducers. The formulation and solution of the Green's integral equation for the inducer problem is found to be very similar to the rotor only problem of a water-jet system. The circulation and pressure distributions on the inducer blade sections are found to be in good agreement with experimental results and RANS calculations obtained using FLUENT. The panel method is also utilized to predict the cavity shapes on the inducer blade.

5.2 Future work

There are multiple avenues for advancing and improving the present numerical method. A few of them are listed in this section.

In reality, the rotor and stator blade geometries have blunt trailing edges. The present panel method can be modified to handle blunt trailing edges by adopting the approach given by Purohit (2013) which obtains a non-lifting sharp extension for finite trailing edges and includes the three dimensional geometry effects when coupling with XFOIL.

The effects of viscosity on the rotor and stator blades can be included by coupling the present panel method with XFOIL to solve the water-jet system. The present panel method needs to be extensively analyzed for cavitating water-jet systems and used to predict the thrust and torque breakdowns as given in Chang (2012).

The present panel method can also be extended to replicate the unsteady interaction between the rotor and the stator using the method developed by He (2010) and Tian (2013). The water-jet propulsion system also needs to be analyzed for unsteady inflows.

Appendix

Appendix 1

Formulation of 2D and 3D Influence Coefficients

The definitions of the dipole and the source influence coefficients for the 2D and 3D panels are listed here.

1.1 2D Influence Coefficients

- Dipole

$$A_{ij} = \frac{1}{2\pi} \int_S \frac{\partial \ln r}{\partial n} ds \tag{1.1}$$

- Source

$$B_{ij} = \frac{1}{2\pi} \int_S \ln r ds \tag{1.2}$$

  where ds is the elemental length.

1.2 3D Influence Coefficients

- Dipole

$$A_{ij} = \frac{1}{4\pi} \int_S \frac{\partial (1/r)}{\partial n} ds \tag{1.3}$$

- Source

$$B_{ij} = \frac{1}{4\pi} \int_S \frac{1}{r} ds \tag{1.4}$$

where ds is the elemental surface area.

Bibliography

[1] S. Brewton, S. Gowing, and J. Gorski. Performance predictions of a waterjet rotor and rotor/stator combination using rans calculations. In *Proc. 26th Symposium on Naval Hydrodynamics*, Rome, Italy, 2006.

[2] S.H. Chang. *Numerical Simulation of Steady and Unsteady Cavitating Flows inside Water-jets*. PhD thesis, Department of Civil Engineering, UT Austin, August 2012.

[3] H. H. Chun, W. G. Park, and J. G. Jun. Experimental and cfd analysis for rotor-stator interaction of a water-jet pump. In *Proc. 24th Symposium on Naval Hydrodynamics*, Fukuoka, Japan, 2002.

[4] M. Drela. XFOIL: An analysis and design system for low Reynolds number airfoils. In *Lecture Notes in Engineering (Volume 54, Low Reynolds Number Aerodynamics)*, New York, 1989. Springer-Verlag.

[5] L. He. *Numerical Simulation of Unsteady Rotor/Stator Interaction and Application to Propeller/Rudder Combination*. PhD thesis, Department of Civil Engineering, UT Austin, August 2010.

[6] J. E. Kerwin. Final report and recommendations to the 25th ittc, specialist committee on cavitation. In *Proc. 25th International Towing Tank Conference*, volume II, pages 473–533.

[7] J. E. Kerwin. Hydrodynamic issues in water-jet design and analysis. In *Proc. 26th Symposium on Naval Hydrodynamics*, Rome, Italy, 2006.

[8] J. E. Kerwin, T. E. Taylor, and G. P. Black, S. D.and McHugh. A coupled lifting-surface analysis technique for marine propulsors in steady flow. In *Proc. Society of Naval Architects and Marine Engineers Propellers and Shafting Symposium*, Virginia Beach, VA, United States, 1997.

[9] M.C. Kim, J.G. Jun, W.G. Park, and H.H. Chun. Flow analysis on the inside of duct for the waterjet system of tracked vehicle with consideration of interaction of rotor and stator. In *Proceedings of Spring Meeting of the Society of Naval Architect of Korea*, Korea, 2002.

[10] S. A. Kinnas, S.H. Chang, and Y.H. Yu. Prediction of wetted and cavitating performance of water-jet. In *Proc. 28th Symposium on Naval Hydrodynamics*, Pasadena, CA, 2010.

[11] S. A. Kinnas and N. E. Fine. A numerical nonlinear-analysis of the flow around 2-dimensional and 3-dimensional partially cavitating hydrofoils. *J. Fluid Mech*, pages 151–181, 1994.

[12] S. A. Kinnas and C.-Y. Hsin. A boundary element method for the analysis of the unsteady flow around extreme propeller geometries. *AIAA Journal*, pages 688–696, 1992.

[13] S. A. Kinnas, H. S. Lee, T. J. Michael, and H. Sun. Prediction of cavitating water-jet propulsor performance using a boundary element method. In *Proc. 9th Int. Conf. on Numerical Ship Hydrodynamics,*, Ann Arbor, Michigan, 2007.

[14] S. A. Kinnas, H. S. Lee, H. Sun, and L. He. Performance prediction of single or multi-component propulsors using coupled viscous/inviscid methods,. In *Proc. 10th Int. Symposium on the Practical Design of Ships and other Floating Structures*, Houston, TX, 2007.

[15] S. A. Kinnas, Alokraj Valsaraj, and S.H. Chang. A panel method for the hydrodynamic performance prediction of a water-jet and an inducer. In *Propeller and Shafting Symposium 2012*, Norfolk,Virginia, 2012.

[16] J. W. Lindau, W. L. Moody, M. P. Kinzel, J. J. Dreyer, R. F. Kunz, and E. G. Paterson. Computation of cavitating flow through marine propulsors. In *Int. Symposium on Marine Propulsors*, Trondheim, Norway, 2009.

[17] L. Morino and C.C. Kuo. Subsonic potential aerodynamics for complex configuration: a general theory. *AIAA Journal*, pages 191–197, 1974.

[18] L. Morino, Chen Lee, and Emil O.Suciu. Steady and oscillatory subsonic and supersonic aerodynamics around complex configurations. *AIAA Journal*, 1975.

[19] J.N.. Newman. Distributions of sources and normal dipoles over a quadrilateral panel. *Journal of Engineering Mathematics*, pages 113–126, 1986.

[20] Jai Purohit. Numerical simulation of ducted propellers. Master's thesis, Department of Civil Engineering, UT Austin, August 2013.

[21] D.D. Scheer. Study of inducer load and stresses. Technical report, NASA, December 1970.

[22] H. Sun and S. A. Kinnas. Simulation of sheet cavitation on propulsor blades using a viscous/inviscid interactive method. In *Proc. 28th Symposium on Naval Hydrodynamics*, Wageningen, Netherlands, 2006.

[23] T. E. Taylor and J. O. Kerwin, J. E.and Scherer. Water-jet pump design and analysis using a coupled lifting-surface and rans procedure. In *Proc. Int. Conf. on Water-jet Propulsion, The Royal Institution of Naval Architects,*, London, UK, 1998.

[24] Ye Tian and S. A. Kinnas. A numerical method for the analysis of unsteady cavitating rotor and stator interaction. In *Third International Symposium on Marine Propulsors*, Launceston, Tasmania, Australia, 2013.

Vita

Alokraj Valsaraj was born in Kannur, Kerala, India along with his twin brother Amithraj Valsaraj on 30th November 1988, the son of R.Valsaraj and P.Lathika. He recieved the Bachelor of Technology in Naval Architecture and Ocean Engineering from Indian Institute of Technology Madras in July 2011. In August 2011, he started his graduate studies as a member of the Ocean Engineering Group at The University of Texas at Austin.

Permanent address: 15000 Park Row, Apt 228
Houston, Texas 77084

This thesis was typeset with LaTeX[†] by the author.

[†] LaTeX is a document preparation system developed by Leslie Lamport as a special version of Donald Knuth's TeX Program.